DUAL PROJECTION FRINGE PROJECTION PROFILOMETRY

by

Bhanu teja Venkatesh

A thesis submitted to the faculty of
The University of North Carolina at Charlotte
in partial fulfillment of the requirements
for the degree of Master of Science in
Mechanical Engineering

Charlotte

2019

Approved by:

_____
Dr. Falaggis Konstantinos

_____
Dr. Rosario Porras-Aguilar

_____
Dr. Edward Morse

ABSTRACT

BHANU TEJA VENKATESH. Dual projection fringe projection Profilometry.
(Under the direction of Dr. KONSTANTINOS FALAGGIS)

Fringe-pattern projection (FPP) techniques are widely used for surface-shape measurement in a wide range of applications like object and scene modeling, part inspection, and reverse engineering. This thesis presents a way to increase the accuracy of FPP and also two ways to accurately perform gamma correction for any projector. The Fringe projection profilometer is build using two projectors and one camera. Although Fringe-pattern projection techniques have been researched in various ways, we are proposing using two projectors which would solve the problem of self-occluding shadows due to discontinuities are solved efficiently. This system can accurately measure a surface which has various applications especially in additive manufacturing, where material is deposited layer by layer and this system can accurately monitor how much material is being deposited in the focused area. A crucial challenge while using projectors in Fringe Projection profilometer is gamma non-linearity, two ways of calibrating the gamma and correcting them have been introduced. This problem is quite common with displays and projectors where the gamma value is modified and used for general purposes, but it is not ideal to use for measurement techniques.

ACKNOWLEDGEMENTS

First and foremost, I would like to express my extreme gratitude towards my research advisor Dr. Konstantinos Falaggis, who has been a very encouraging, motivating and understanding advisor. He has provided with excellent guidance and path for my research and also for providing with all the materials needed for competition of this thesis. His zeal for excellence and perfection is highly infectious and has helped me bring the project to this level of completion. I would also like to thank Dr. Rosario Porras-Aguilar for her constant support in any kind of equipment usage in her lab in the initial testing days. I would like to thank Mr. Jeffrey Raquet for getting the 3D-printed parts in very short periods of time. I would also like to thank Dr. Jerre M. Hill for helping with finding lab equipment whenever I had shortage of some materials. I would also like to extend my thanks to Ana Hiza Ramirez-andrade for being a great lab partner and helping out with some equipment and occasional software issues. I would like to thank Abhinav Mishra for being a great friend and lab partner throughout my thesis period and even with finish up with this report. I am grateful for my parents for their support emotionally and financially without them this would never have been possible. I am also thankful to Swathi who was with me all along this project until the time of helping with the report. This work was supported, in part, by funds provided by the University of North Carolina at Charlotte. Last, my thanks also goes to all the staff of Mechanical Engineering and Engineering Science department in William States Lee of Engineering college. With their support I had a happy time during the research work at the University of North Carolina at Charlotte.

TABLE OF CONTENTS

LIST OF FIGURES

CHAPTER 1 : INTRODUCTION

1.1 Statement of Intent

Real time measurement data of each layer deposited in Additive Manufacturing process is a challenging problem which can be solved using Fringe Projection techniques. Additive Manufacturing has a wide range of applications in many industries. Especially in areas demanding extreme precision like space applications and complex machinery in automobiles etc. Due to the challenging nature of the problem the manufacturing of the machines is trusted and is finally measured once the product is finished for quality check. The objective of this thesis is to develop such method that can be scaled according to the machine, it will open up a new area of quality control for such machines.

The motivations of this research are introduced in section 1.2. Related works are reviewed in section 1.3 and the structure of this thesis is introduced in section 1.4.

1.2 Motivations

1.2.1 Additive Manufacturing

Additive Manufacturing is a common name for a series of processes that are recognized by being computer controlled, highly automated, and manufacture objects by a layered deposition of material. Additive Manufacturing, a fairly new palette of manufacturing technologies since 1989 had an annual growth rate of 32% [1] and is predicted to be one of the main driving forces towards an era of digital manufacturing. The palette of processes, in common tongue affectionately designated 3D printers, is regarded upon by many as science fiction turning science fact. Machines that to some extent already can a universally will be able to procure any object, any one thing that can be imagined. Today, readily finished products (restrained to one material) can be built directly on

additive manufacturing equipment. Tissue Engineering using Additive Manufacturing allow organs and tissue to be Additively manufactured from the patient's own living cells [2]. 3D printers in conjunction with a 3D scanner becomes a 3D photocopier Amazing is that geometries can be made by additive manufacturing to a complexity and level of detail so high, that not even highly advanced industrial measuring techniques can measure and verify the geometrical freedom given.

With a field of technology in such rapid growth, there are many open-ended questions awaiting to be answered, and many areas of the field to which research will fuel development and immediately impact the industry. An area particular interest is addressed within the scope of this Thesis. This will improve the quality of the Manufactured product when integrated with 3-D printers and reduce faulty products which are not usable. This will help Additive Manufacturing technologies reach one step closer to becoming the autonomous, digital manufacturing method of tomorrow.

1.3 Topic Overview

Although we have come quite far in advancing 3-D printing techniques, the goal is to develop such a method which can track how much material is being solidified using different methods in additive manufacturing process. The more intricate the machine is the more crucial parts it will manufacture. Which requires a high detail of precision and certainty in the product being manufactured. These manufacturing methods deposit the raw material layer by layer which are often less than 1mm. This thesis aims to develop a method to track this thin layer.

Before going more into detail, it is important to understand where fringe projection methods stand in relation to the other three-dimensional measurement

techniques. Fringe projection methods belong to the category of non-contact approaches, in opposition to contact methods that require scanners to probe the subject through physical touch, like for example the CMM (Coordinate Measuring Machine). Within the non-contact methods there are two main categories, the passive and the active methods. Techniques that are not based on controlling the emission of any kind of radiation themselves and instead rely on detecting reflected ambient radiation are known as passive. There are types of noncontact active methods that make use of ultrasound waves or methods that make use of magnetic resonance, as in the case of MRI (Magnetic resonance imaging). On the other hand, the fringe projection method, is one of the active methods that revolves around the emission of structured light on objects and detecting its reflection. Structured light systems can follow one of two approaches, whether they use single shot techniques like the rainbow 3D camera [3][4][5], and the continuously varying color code technique, or multi-shot methods as in the case of binary coding, gray coding phase shifting[6][7][8] and the hybrid gray coding and phase shifting.

This research uses the multi-shot phase shifting method as it is the main three-dimensional measurement technique. Phase shifting is a well-known fringe projection method for surface imaging that uses a set of sinusoidal patterns projected onto a surface, and a digital camera to capture the phase difference (between the original pattern and the captured one) modulated by the topography of the object to extract information about the depth of the object for each pixel of the captured image. In order to obtain this information, phase modulation analysis computes the phase of the captured light. However, the phase obtained is not its absolute value, but only its integer multiple of 2π value (2π by considering that the phase is measured in radians), as the object surface often introduces

phase shifts on the pattern that are superior than 2π [9]. In other words, it is only measured the remainder of the division of the phase by 2π, the so-called wrapped phase. From the wrapped phase it is only possible to obtain depth measurements that correspond to phase shifts in the interval of $[-\pi, \pi]$. To solve this problem, phase unwrapping, the process that converts the wrapped phase into absolute phase, is required. This will be explained in detail further in Chapter 2.

1.4 Objective

We choose a range of 1mm to analyze fringe patterns from two projectors and measure the phase that is sent from the projector and measure this phase on a flat object which should be ideally the same as sent phase. We increase the distance of the object by 1/50 mm in Z direction 20 readings are taken by one projector. The readings mean the Phase in X-direction and Phase in Y-direction. These readings when 3-D plotted would give an idea of how the volume varies with respect to Z direction which can be used to measure the layers deposited accurately without any errors as the deviation of volume in Z direction is already accounted for. The main objective is to be able to map a function which can help in measuring objects in Z direction. Measuring objects in X,Y direction was very well accomplished in Fringe Projection Techniques.

1.5 Structure of the Thesis

This Thesis is divided into five chapters. Chapter one addresses the wide scope of the additive Manufacturing process and what problems would be solved in this thesis, Motivation for choosing Additive Manufacturing process as the application for this Fringe projection Technique and a topic overview and objectives of this thesis. Chapter two introduces what Fringe projection Profilometry is and the methods that are available

to be used and which method is selected and why. Chapter three introduces the hardware system used, the specifications of them and the design prior to the assembly in CAD. Chapter four is focused on the MATLAB simulator and how the readings were taken. This chapter also presents the results obtained . Finally, the chapter five succinctly draws conclusions about the results obtained setting some future research directions.

CHAPTER 2 : OPTICAL METROLOGY THEORY

2.1 Introduction

The field of non-destructive testing and analysis is a widely used method in the field of metrology and optical metrology plays a very important role in this method. Optical measurement techniques make it possible to obtain important visual information under difficult conditions such as boilers or in sensitive environments, where precision is required. These techniques can be categorized into two main areas based on the type of measurement. The first category includes techniques, which provide information on the shape or structure of the test object while the other category includes techniques that analyze properties of the object other than its shape [10]. Some examples of applications in the first category are surface roughness measurements, inspection and measurement of wafer surface during VLSI manufacturing and shape recognition. The second category supports applications that go beyond plain visual inspection, such as material characterization, coating evaluation, detection of overheated components[10]. Further sections in this chapter will cover some of the techniques used for surface inspection and the technique selected in this thesis.

2.2 3D Profilometry

Non-contact 3D profilometry techniques have become increasingly popular because of its superior features. Non-contact profilometry usually employs light as means of measurement. Systems based on such technology allow object surfaces to be soft or fragile. This allows for the objects to be measured without being contaminated[11]. Furthermore, non-contact acquisition techniques can achieve very high-speed and precise

measurement. Some approaches can be applied in real time applications. However, these techniques also have their limitations; they have relatively strict requirements on optical characteristics of the target surface. But these requirements do change according to the Measurement Technique selected.

2.3 Projection based Measurement Techniques

Fringe projection is a simple way of contouring in which interference fringes are projected onto the object under test at a given angle and are viewed from a different angle. It is a convenient technique for contouring objects with too great a height variation to be measured with standard interferometry. Two variants of fringe projection technique, namely *fringe projection with coherent light* and *fringe projection with incoherent light* can be implemented, based on the type of illumination and fringe generation technique. These are explained in detail in the following sections.

A Fringe-Pattern Projection system typically consists of a digital projector, computer with an image capture capability, and a camera (Fig. 2.1). A computer is used to generate the several phase-shifted fringe patterns and controls the switching between the different phase-shifts. The projector is used to project the phase-shifted fringe patterns onto the object surface. A digital camera captures each of the projected phase-shifted fringe patterns. From the camera's perspective, the fringe patterns appear distorted according to the topography of the object. Once the camera has captured each of the phase-shifted images, the height (depth) of the object can be computed for each pixel using the method and equations discussed in Section 2.4 or 2.5, for the sinusoidal and triangular patterns, respectively.

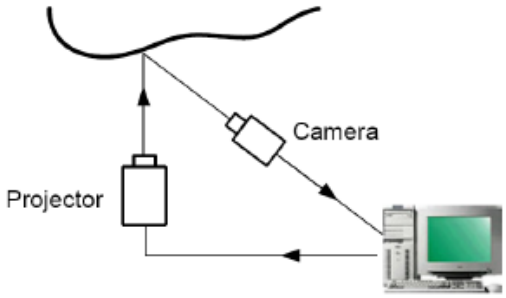

FIGURE 2. 1 : A Basic Fringe Projection System Schematic[12]

2.3.1 Fringe Projection with Coherent Light

When a sinusoidal intensity distribution is projected on a surface, the mathematical representation of the deformed grating image intensity distribution is similar to that obtained in conventional interferometry. The surface height distribution can be translated to a phase distribution, which can be obtained by means of Fourier transform analysis.

A sinusoidal intensity distribution can be projected on the surface of interest by generating an interference pattern between two coherent plane wave fronts. In coherent light fringe projection, a laser source in conjunction with an interferometer such as a Michelson interferometer is used to generate the interference fringes to be projected[13]. The fringe spacing p is given by

$$P = \frac{\lambda}{2 \sin \theta} \qquad (2.31)$$

Here λ is the wavelength of illumination and 2θ is the angle between the two interfering beams, as shown in Figure 2-1. From Eqn. 2.31, we can see that simply by tilting one beam with respect to another, the fringe period can be changed. The larger the angle between the two beams, the smaller will be the fringe period.

For geometrical analysis of a fringe projection system [13], consider two plane waves with propagation vectors and incident on a surface S_1 whose height distribution is to be determined. This results in an interference fringe pattern being projected on the surface. Let the surface height be described by a function $z_1=f_1(x, y)$. This is shown in Figure 2-1.

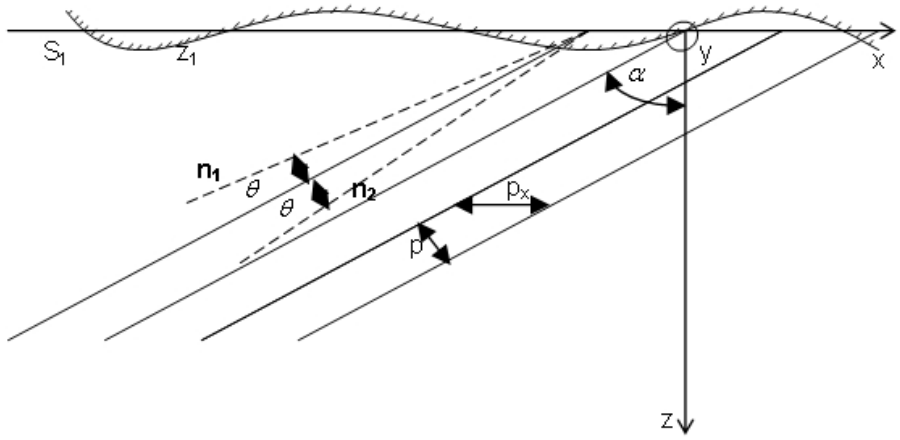

FIGURE 2. 2: Analysis of fringes with fringe spacing 'p' projected at an angle α on the surface under test [13]

For geometrical analysis of a fringe projection system[13], consider two plane waves with propagation vectors $\overrightarrow{n_1}$ and $\overrightarrow{n_2}$ incident on a surface S_1 whose height distribution is to be determined. This results in an interference fringe pattern being projected on the surface. Let the surface height be described by a function $z_1=f_1(x, y)$. This is shown in Figure 2.2.

The two waves in the directions $\overrightarrow{n_1}$ and $\overrightarrow{n_2}$ and lie in the xz-plane making an angle to each other and the line bisecting 2θ makes an angle α to the z axis. The two incident waves have equal intensity I_0. The intensity distribution across the surface is found as

$$I_1(x,y) = 2I_0(x,y)[1 + cos\frac{2\Pi}{p}(x\,cos\,\alpha + z_1\,sin\,\alpha)] \quad (2.32)$$

where the distance p between the fringes is as defined in Eqn. 2.31. Eqn. 2.32

For moderately curved surfaces, Eqn. 2.32 can be regarded as a phase-modulated sinusoidal grating with the spatial period

$$p_x = {}^{p}/_{cos\,\alpha} \quad (2.33)$$

which corresponds to the spatial frequency

$$f_{cx} = {}^{1}/_{p_x} = \frac{cos\,\alpha}{p} \quad (2.34)$$

and the spatial phase modulation function

$$\psi_1(x,y) = z_1\frac{sin\,\alpha}{p} = f_1(x,y)\frac{sin\,\alpha}{p} \quad (2.35)$$

where $z_1 = f_1(x, y)$ describes the surface.

Hence, Eqn. 2.32 changes to

$$I_1(x,y) = 2I_0(x,y)\left\{1 + cos2\,\pi[\frac{x}{P_x} + \psi_1(x,y)]\right\} \quad (2.36)$$

A practical way of applying this method is sketched in Figure 2.3 where the two plane waves are formed in a Michelson interferometer with a small tilt of one of the mirrors.

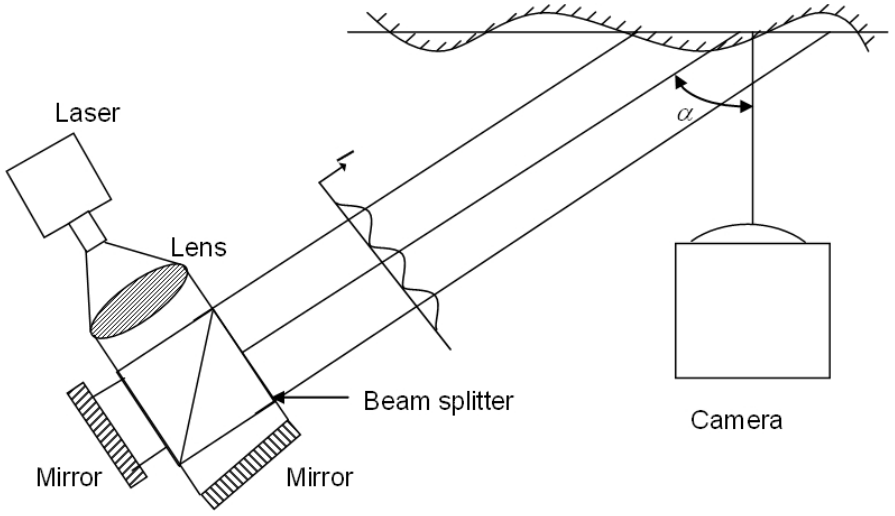

FIGURE 2. 3: Fringe projection using a coherent light source[13]

The camera placed along the z-axis captures the surface with the projected fringe pattern. The resulting intensity I_1 captured by the camera is given by Eqn. 2.36.

2.3.2 Fringe Projection with Incoherent Light

In the case of incoherent light fringe projection, the light source is changed to a white light source. White light is the term used to describe the low coherence nature of the light sources, such as LEDs, used in such a technique. Since it is much more difficult to observe interference between waves generated from such sources, the fringe generation technique is modified. A structured light pattern is projected onto a lens system to obtain a telecentric light

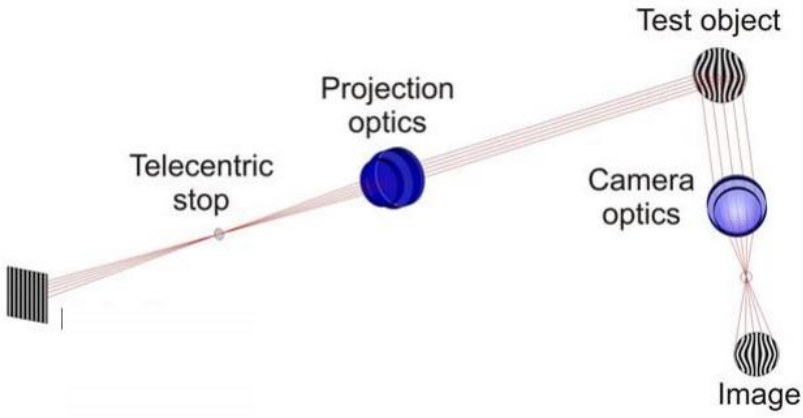

FIGURE 2. 4: Figure showing use of lens systems to make the light from the projector telecentric. [14]

2.4 Sinusoidal fringe-pattern projection

The general expression for the distorted sinusoidal-intensity fringe pattern (Fig. 2.4) observed by a camera after being projected onto an object surface is as follows[15]:

$$I_i(x,y) = a(x,y) + b(x,y)\cos[\phi(x,y) + \delta_i],\ i=1,2,3....N \qquad (2.37)$$

The three unknowns, *a(x; y)∈[0; 1]*, *b(x; y) ∈ [0; 1]*, and ϕ(x; y) are respectively: the background intensity, amplitude of modulation, and phase at each image coordinate *(x, y)*. The phase map, ϕ *(x, y)*, contains the depth information of the object[15]. This unknown map with N phase shifts indexed by *i* is solved using the following:

$$\phi(x,y) = -arctan\frac{\sum_{i=1}^{N} I_i(x,y)\sin\delta_i}{\sum_{i=1}^{N} I_i(x,y)\cos\delta_i} \qquad (2.38)$$

The gray level intensity of the *i*th phase shift, $I_i(x, y)$, is detected by the CCD camera and δ_i is the phase shift, expressed according to the following[15]:

$$\delta_i = \frac{2\pi i}{N}, \qquad i = 1,2,3,\ldots.\mathrm{N} \qquad (2.39)$$

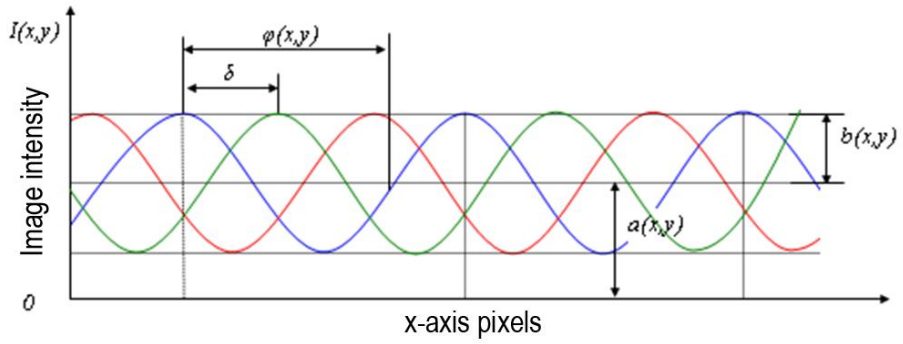

FIGURE 2. 5: Sinusoidal Pattern with three phase shifts 120^o apart [15]

The minimum number of phase shifts required when using a sinusoidal pattern is three, one for each unknown. Thus, three equations in the form of Equation 2.37 are needed. The three patterns are sequentially projected by the projector and then captured by the camera. In the case when N = 3, there are several possible phase-shifts. The best accuracy is obtained when each phase shift is separated by 120^o [16]. Equation 2.38 can then be simplified to:

$$\phi(x,y) = -arctan\left(\frac{\sqrt{3}I_3(x,y) - I_2(x,y)}{2\,I_1(x,y) - I_2(x,y) - I_3(x,y)}\right) \qquad (2.44)$$

This yields the wrapped phase map $\phi(x, y)$ between 0 and 2π. The continuous phase map is obtained through a phase unwrapping[15][16], algorithm which will be explained in further in this chapter.

2.5 Triangular fringe-pattern projection

The triangular fringe pattern (Fig. 2.6) has the advantage of requiring less processing than the more traditional sinusoidal fringe pattern[19]. This is because the minimum number of image acquisition steps is only two rather than the three needed for the sinusoidal fringe pattern. It also uses an intensity-ratio rather than the phase. Intensity ratio is less expensive to compute since it does not use the arctangent function as in Equation 2.51[20]. The N-step general expression for the projected triangular intensity fringe pattern is as follows[21]:

$$I = \begin{cases} \frac{2I_m(x,y)}{T}(x+\delta_i) + I_m(x,y) + \frac{I_m(x,y)}{2} & x+\delta_i \epsilon [0, \frac{T}{4}) \\ -\frac{2I_m(x,y)}{T}(x+\delta_i) + I_{min}(x,y) + \frac{3I_m(x,y)}{2} & x+\delta_i \epsilon [\frac{T}{4}, \frac{3T}{4}) \\ \frac{2I_m(x,y)}{T}(x+\delta_i) + I_{min}(x,y) - \frac{3I_m(x,y)}{2} & x+\delta_i \epsilon [\frac{3T}{4}, T) \end{cases}$$

$$I_m(x,y) = I_{max}(x,y) - I_{min}(x,y) \qquad (2.51)$$
$$= 2b(x,y)$$

where $I_m(x, y)$ is the difference between the maximum $(I_{max}(x, y))$ and minimum ($I_{min}(x, y)$) intensities; T is the pitch or period of the pattern and δ_i is the shift according to Equation 2.52

$$\delta_i = (i-1)\frac{T}{N}, \qquad i = 1,2,\ldots\ldots,N \quad N \geq 2 \qquad (2.52)$$

Using more than the minimum number of steps improves the accuracy of the measurement at the expense of additional processing time for the additional images to

be captured. To compare the effect of saturation on the number of steps, the triangular 3-step method is used in addition to the 2-step pattern for the analyses presented in this thesis. The equations for the intensity ratio $r_0(x, y)$ using the two-step[22] and three-step[20] triangular phase-shifting algorithm are shown in Equations 2.53 and 2.54, respectively. In the case of the 3-step equation, $I_{high}(x, y)$, $I_{med}(x, y)$, and $I_{low}(x,y)$ are respectively the highest, median, and lowest captured intensity at each image coordinate (x, y) of the three phase-shifted images.

$$r_0(x,y) = \frac{|I_1(x,y) - I_2(x,y)|}{I_m(x,y)} \tag{2.53}$$

$$r_0(x,y) = \frac{I_{high}(x,y) - I_{med}(x,y) + I_{low}(x,y) - I_{min}(x,y)}{I_m(x,y)} \tag{2.54}$$

The result from Equation 2.53 or 2.54 is wrapped from 0 to 2N. This is shown in the cross-section of triangular pattern for the 2-step and 3-step algorithms along with the wrapped and unwrapped intensity ratio in Figure 2.6.

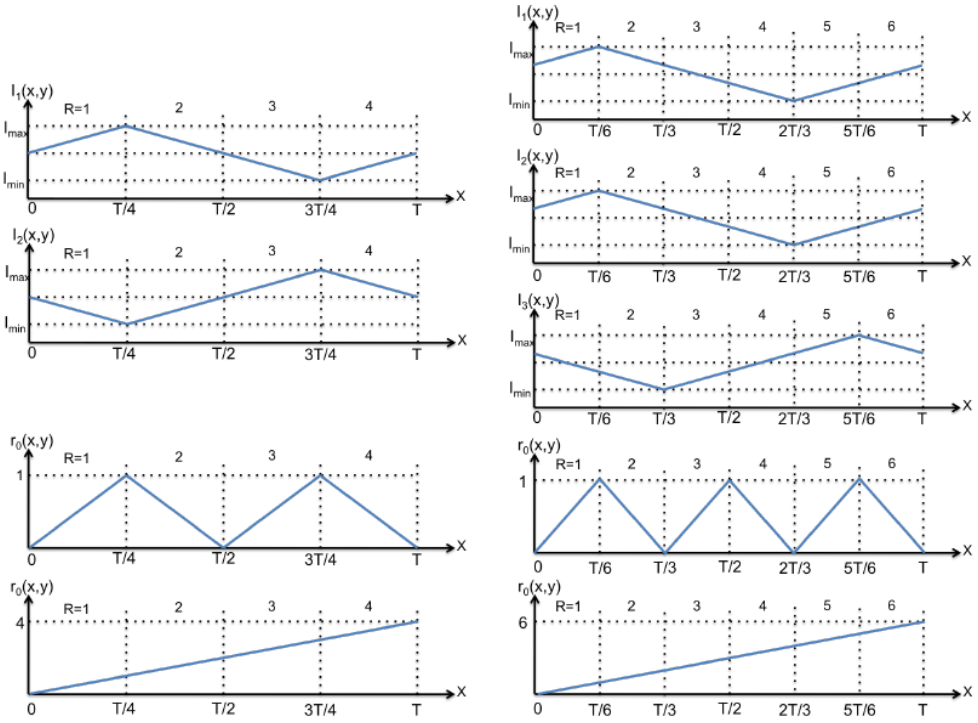

FIGURE 2. 6: Cross-section of triangular fringe pattern: In the left column is the 2-step phase-shifted patterns while in the right column are the 3-step phase shifted patterns. The intensity ratio and the unwrapped intensity ratio are shown respectively under their set of phase-shifted patterns.(Adapted from[19])

2.5 Phase Unwrapping

Phase wrapping is a process whereby a real-valued surface, $\phi(s)$, is wrapped into the interval $[\pi, \pi)$ by the following operation:

$$W\{\phi(s)\} = \psi(s) = \phi(s) + 2\pi k(s)$$

where k (s) is an integer function that forces $\pi \leq \psi < \pi$. For the two-dimensional case, s = (x, y). We assume that the measurements are sampled on a rectangular equidistant grid, as is typical in practical applications[23]. Accordingly, we denote

$\psi_{i,j} = \psi(x_i, y_j)$ and $\phi_{i,j} = \phi(x_i, y_j)$ with

i = 0,1,2,…..M, j = 0,1,2,…..N

Unwrapping is the process of estimating the actual function, ϕ, from the wrapped function, ψ. We say that a candidate reconstruction, ϕ, is feasible if $W(\phi) = \psi$. Constraints must be placed on the choice of ϕ, since any two surfaces that differ point-wise by some integer multiple of 2π are feasible solutions[12]. The most common approach is to seek the "smoothest" possible unwrapped estimation. According to this smoothness criterion, unwrapping algorithms try to minimize some norm of the discontinuities in the reconstructed surface. A discontinuity is defined by a pair of neighboring pixels whose difference exceeds π in magnitude. Often, a user defined weighting is associated with each such pairing, to reflect the confidence in the smoothness assumption at the corresponding locations.

2.5.1 Multi-frequency (hierarchical) temporal phase unwrapping

In this method of unwrapping technique, the fringe pattern with different fringe densities are projected, and the coarsest fringe pattern has only one fringe in all, of which the phase without any 'wraps' (because its values do not exceed the range of $[-\pi,\pi]$) is then used as fundamental information for further phase unwrapping. The other phase maps are unwrapped based on their previous unwrapped phase maps one by one according to the relation of their frequencies or fringe numbers. Since the phases are unwrapped from the coarsest layer to the finer ones, this sorting method is also well known as 'hierarchical' unwrapping approach[24]. Different from spatial unwrapping techniques, Temporal Phase Unwrapping(TPU) is performed in the time domain for each pixel by using the wrapped phase images calculated for each of the varied fringe densities, shown in Fig. 2.7. Consequently, pixels are not affected by poor signal to noise ratios in neighboring pixels, as often seen in spatial unwrapping techniques.[25]

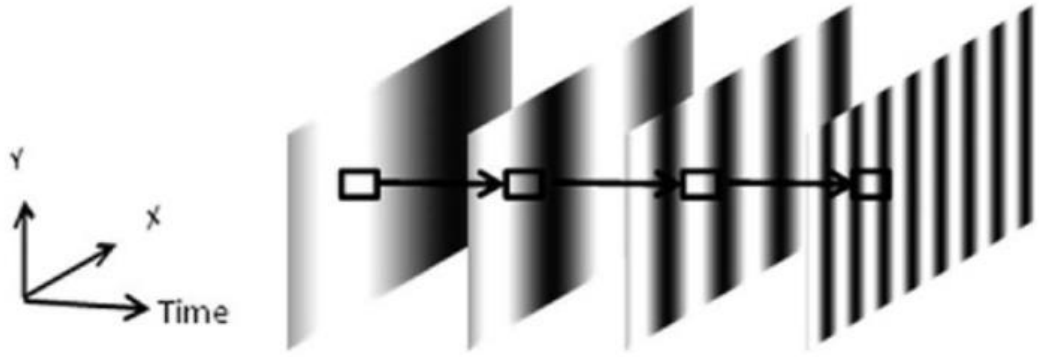

FIGURE 2. 7 : Temporal phase unwrapping is executed along the time axis, with increasing fringe frequency.[26]

This hierarchical approach to unwrapping is based on following an increasing fringe frequency starting with no discontinuities in the phase map [26].Mathematically, the unwrapped phase, u, of a particular image can be calculated as follows:

$$u\Phi_{i+1}(x,y) = \Phi_{i+1}(x,y) + 2\pi N_{i+1} \pm \varepsilon$$

Where Φ represents the wrapped phase and N is the fringe order number that characterizes phase jumps with the addition or subtraction of integer values; thus, images are corrected and have no phase jump discontinuities. An error term, ε, is added due to electrical noise and effects of uncertainties in the algorithm. A particular resolution can be reached by determining how the error term propagates through varying numbers of images used to recover the unwrapped phase. Figure 2.8 shows how the error is minimized as more images are used in the TPU [27].

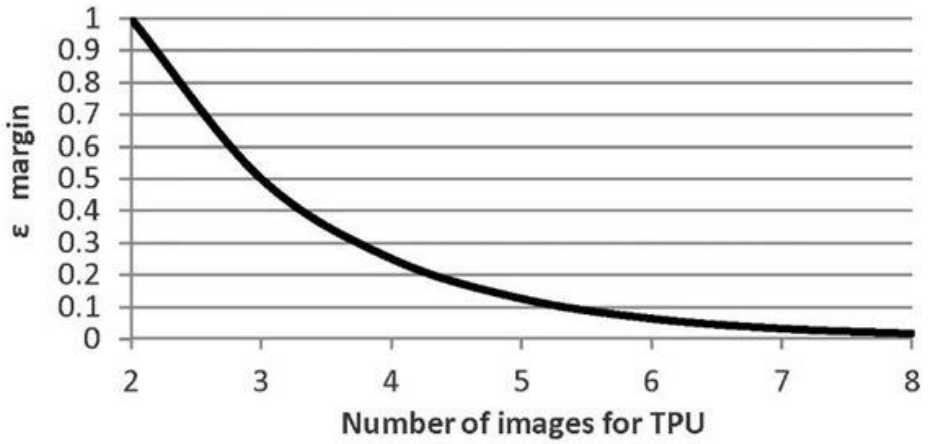

FIGURE 2. 8: Error propagation as a function of the number of images used in the temporal phase unwrapping algorithm. [27]

Although the error approaches zero, the maximum fringe frequency is limited to the DMD pixel. Thus, higher resolutions can be achieved by using more images in the unwrapping algorithm in situations where time is not a critical factor. The TPU unwrapping sequence can be determined based on the particular application and its requirements[27].

2.6 Selection of Technique

The choice of the most appropriate technique for the system was based on our requirement for a system suitable to eliminate and smooth out shadowing and shiny effects due to the angle of projection and the type of projector used. Thus, it was important for the technique and the hardware to be in synchronization with each other. We have chosen the Fringe projection profilometry using incoherent light source to illuminate an object size of up to 6 x 8 cm. This method allows us to illuminate a wide array of objects. Another important requirement was the need to measure any height variations in order to map the height of the object. We need to measure large height variations (0.1- 10 mm) . Standard

interferometry is able to detect surface height variations on the order of a few wavelengths of the laser used for measurement.

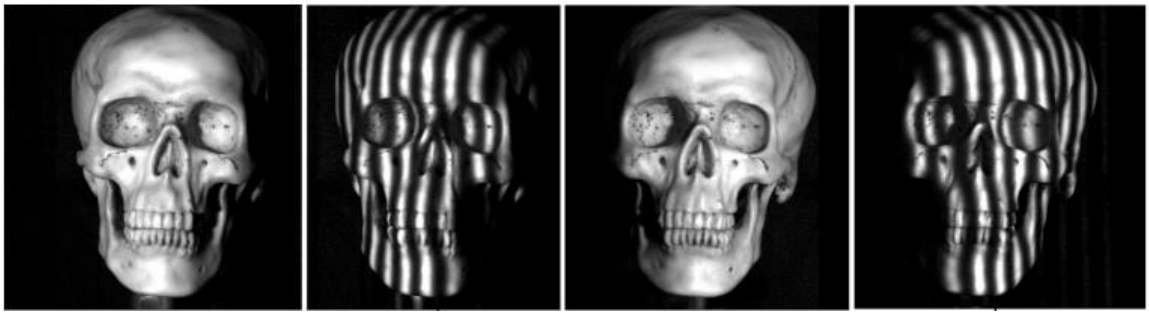

FIGURE 2. 9: Here we show the plastic human skull from the two projectors' perspectives. The first two pictures show light emitted and the shadows on right side of the skull due to the projector on left side and the last two pictures show light emitted and shadows on left side of the skull due to the projector on the right side.(adapted from [28])

For surfaces, which have much larger height variations, the classical interferometry techniques fail to perform well, and we need to utilize other techniques such as fringe projection, moiré interferometry etc. Among these two, we selected the fringe projection technique for its ease of implementation. As our main goal is to eliminate any missing data due to shadows and reflective surface, we further have chosen a dual projector Fringe projection profilometer which uses 2- projectors and 1-camera and can digitize discontinuous solids with diffuse light surface. This Fringe projection profilometer solves the self-generated shadows cast by the object discontinuities due to the angle between the camera and the single white-light fringe projector in standard profilometry. For example, to understand this in an easy way, if we look at the Figure 2.9 where the first two images are from a projector placed on the left side of the skull. In these two images the first image has just normal light projected, and the second image has the fringes, and we can see some shadows on the right side of the skull where some of the light is unable to reach. This is the problem even when the projector is placed on the right. If the projector is placed in the

center there would be shadows on the edges of the skull. The result of these shadows would be loss of data in those areas. In order to avoid this, both the projectors are used one after another and any missing data would be compensated by the other projector. Similarly, the loss of data occurs with reflective surfaces as well due to surface glare.

CHAPTER 3: DESIGN AND HARDWARE SYSTEM SETUP

3.1 Overall System Description

The basic concept is to develop a system to overcome shadows that occur due to various constraints like the angle of the projected light. The optical system has been implemented after careful optical calculations which will be further discussed in this chapter. The optical system is implemented on an optical base plate of size "50x50", consisting of a solid aluminum plate, anodized black and tapped with ¼-20 holes. The key optical and imaging components of the system are mounted on this base plate. DLP Lightcrafter 4500 is the projector that is used. The camera used is a Pointgrey camera. In addition to these main parts, the system requires many other accessories such as power supply adapters for the light source, camera adapters, lens and lens mounts.

The in-built lens system of the Lightcrafter 4500 is removed due to its limited range, lack of detailed information of the type of lens system used and collimating the light was not possible. So, the in-built system is replaced with a simpler single lens. The projector when used by itself, the light will expand as we move the object away from the projector. This can lead to inaccurate measurement. So, this is eliminated by using an aperture stop after the replaced lens. The aperture will only allow parallel light rays to pass through . This is followed by another lens of size 4 inch in diameter, this lens is the limiting factor for the size or range of the object that can be measured. Once light passes through this, the light obtained is highly collimated.

3.2 Hardware Components

- DLP light crafter 4500
- 3-D printed Housing for the Projector
- Imaging Source Camera (DMK 33GP5000e)
- Lens for the camera
- 30 mm focal length lens of 18 mm diameter
- 3-D printed mount for the lens
- 300 mm focal length lens of 4-inch diameter
- Lens mounts
- Optical Base
- 2-port HDMI Video Splitter -4k at 60Hz

3.2.1 Digital Micro-mirror Devices (DMD) and DLP Projectors

The DLP concept originated from Texas Instruments(TI) in the later 1980's. In 1996, TI commercialized its first generation of DLP projectors. DLP projectors fundamentally have many advantages over LCD projectors due to digital nature of DLP. The core of DLP technology is an optical switch called DMD [29][30]. DMD consists of an array of tiny mirrors, each operating in a bi-stable mode, tilting diagonally $+\theta$ degrees (ON) or $-\theta$ degrees (OFF) about the hinge attached to the support post. Each microscopic mirror corresponds to one pixel of the light in a projected image. By switching these mirrors ON and OFF up to several thousand times per second, a DLP projection system can translate a digital video or graphic source into a projected image with maximum fidelity. The proportion of time during each video frame that a micromirror remains ON determines the shade of pixel gray scale from black (for 0% ON-time) to white for (100% ON-time).

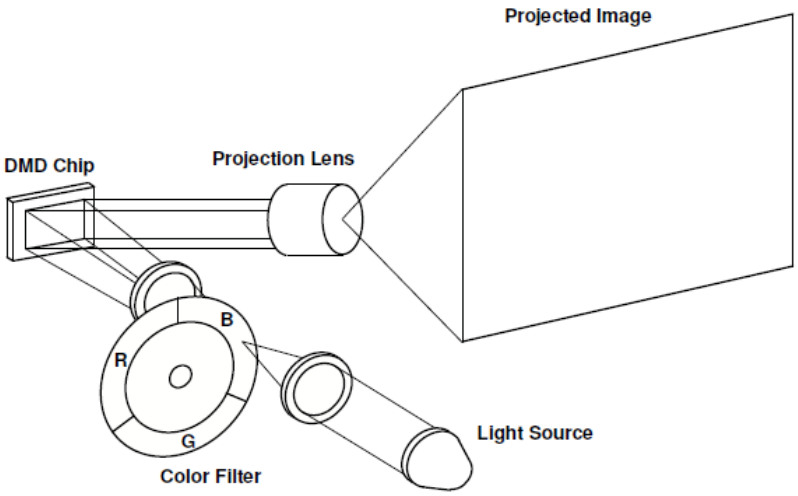

FIGURE 3. 1: Single-chip DLP projection system configuration

Figure 3.1 shows the configuration of a DLP projector with one DMD chip. The light from the illuminator is first focused to a small spot on the color filter. The color filter spins at high speed producing red, green and blue light sequentially that illuminates the DMD surface. The image to be projected is formed on the DMD chip. Since there is only one DMD chip in the projector, but a 24-bit color image is to be projected, the projector operates in a unique color-channel-switching mode. At one specific moment only one channel of the color image, red, green, or blue, is projected and the three-color channels are projected in sequence. A photodiode mounted on the cover of the DMD projection engine monitors the position of the color filter and provides a timing signal to the projector. Based on this signal, the DMD forms the image of the corresponding color channel. Since the color channels are switched at high speed, what the viewer sees is a 24-bit color image.

For a single-chip DLP projection system, the color filter functions as the color generator. The color filter usually contains three or six color segments for sequentially separating red, green, and blue wavelengths. Typically, a white (or clear) segment, which is usually a section of anti-reflection coated glass, is added to boost the brightness of the projected image. The four segments (red, green, blue and clear) of the color wheel does not distribute uniformly. Usually the red segment is the largest and the white one is the smallest, which is used to balance the projected color channels[12]. In comparison with Cathode-Ray Tube (CRT) or LCD displays, DLP displays have their own advantages because they are inherently digital.

1. High image quality. Each DMD device includes up to 1.3 million individually hinge-mounted microscopic mirrors. Its projection image is film-like or video with photographic quality. Since the image produced by DLP projectors is the exact mirror image of its source material, it comes closer than any other display solution to reproduce the source image.
2. Large color range. DLP technology reproduces a range of color up to eight times greater than that of analog projection systems. DLP projection creates rich blacks and darker shades than is possible with other technologies and projects no fewer than 35 trillion colors over eight times more than what is possible with film.
3. Long operation hours. It has been demonstrated that DLP projectors can work reliably over 100,000 operation hours and more than 1 trillion mirror cycles. They are reliable enough and their life expectancy is long enough for the ordinary users.
4. Inherent noise immune. With all-digital displays, users can watch without ground-loop noise or electromagnetic interference from household appliance or local

radiation sources. Unique new features are only possible with digital view processing in the dis- play. Its digital nature matches well with today's surge in computer graphics display.

In summary, DLP projection display technology offers exceptional flexibility, high brightness, high resolution, and high image quality. DLP projectors enable us to generate fringe patterns easily and accurately, which is one of the key factors of our high-speed and high-accuracy measurement research. So, the DLP lightcrafter 4500 was chosen in this thesis. The 3-D printed housing was designed, 3D printed with extreme care and multiple iterations were done to achieve a perfect fit for the projector. Details of 3-D printing are explained in the next section of this chapter. The design, 3-D printing of the projector housing and the lens housing had to be taken care personally and multiple iterations of the printed versions had to be checked to make sure the lens and the projector fits perfectly inside the 3D printed housing.

FIGURE 3. 2: DLP Light crafter 4500 with all components intact

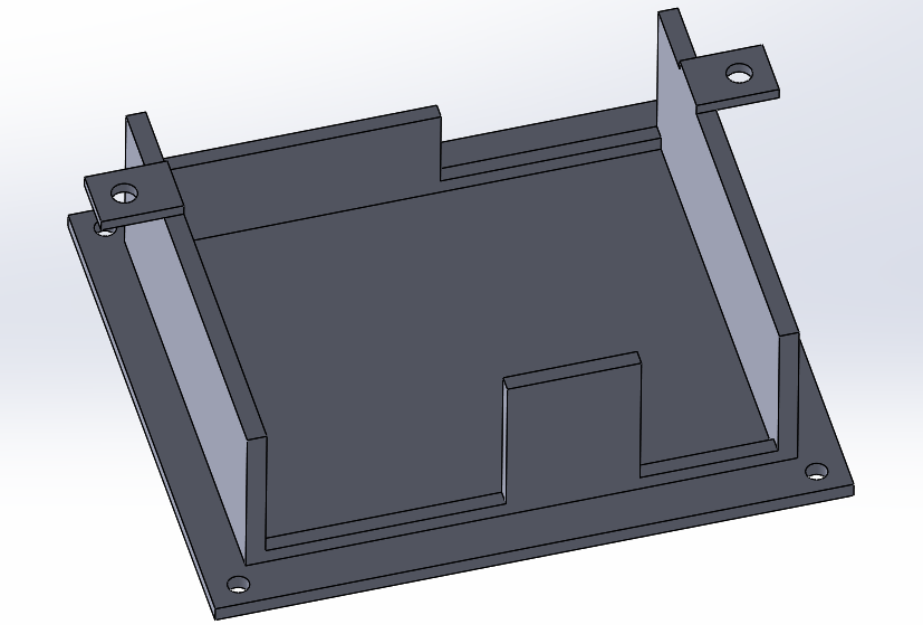

FIGURE 3. 3: CAD model of the projector housing designed in Solidworks

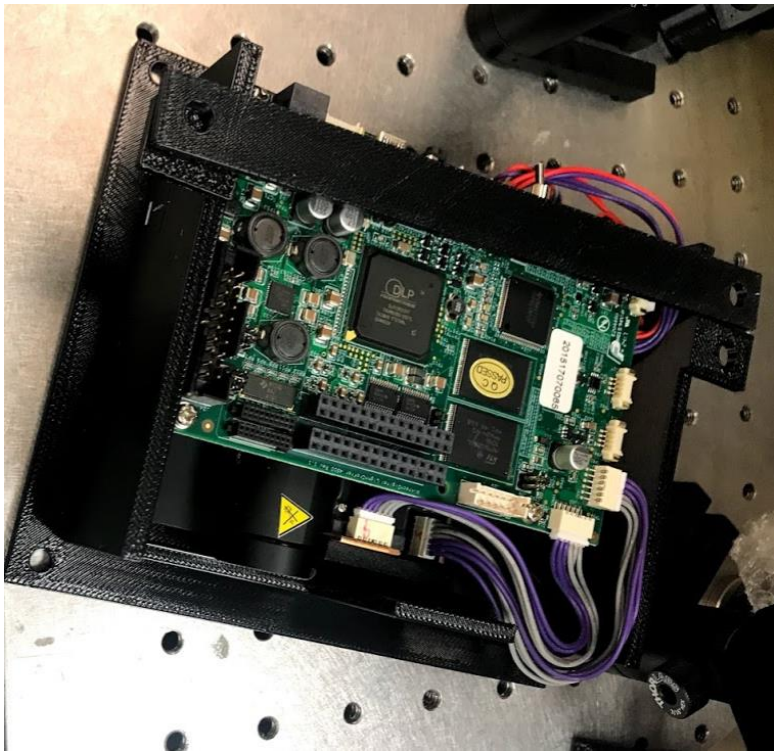

FIGURE 3. 4: Projector inside the 3-D printed Housing

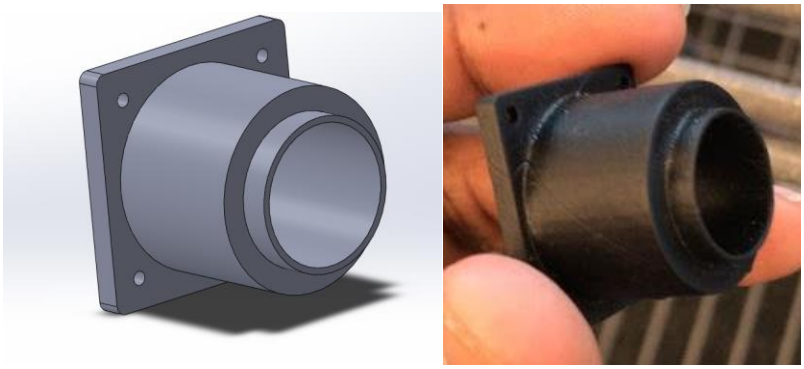

FIGURE 3. 5: The CAD model of the housing of 30 mm focal length lens and the 3-D printed part on the right

3.2.2 3-D Printing

The term 3D printing covers a variety of processes in which material is joined or solidified under computer control to create a three-dimensional object, with material being added together (such as liquid molecules or powder grains being fused together), typically layer by layer. In the 1990s, 3D printing techniques were considered suitable only for the production of functional or aesthetical prototypes and a more appropriate term used was rapid prototyping. Today, the precision, repeatability and material range have increased to the point that some 3D printing processes are considered viable as an industrial production technology, whereby the term **additive manufacturing** can be used synonymously with 3D printing. One of the key advantages of 3D printing is the ability to produce very complex shapes or geometries, and prerequisite for producing any 3D printed part is a digital 3D model or a CAD file.[31]

For the projector used in this thesis, the housing was 3-D printed using FDM. Fused Deposition Modeling (FDM), or Fused Filament Fabrication (FFF), is an additive manufacturing process that belongs to the material extrusion family. In FDM, an object is

built by selectively depositing melted material in a pre-determined path layer-by-layer. The materials used are thermoplastic polymers and they come in a filament form.[32]

FDM is the most widely used 3D Printing technology: it represents the largest installed base of 3D printers globally and is often the first technology people are exposed to. In this article, the basic principles and the key aspects of the technology are presented.

Working of the FDM can be simplified as follows :

1. A spool of thermoplastic filament is first loaded into the printer. Once the nozzle has reached the desired temperature, the filament is fed to the extrusion head and in the nozzle where it melts.
2. The extrusion head is attached to a 3-axis system that allows it to move in the X, Y and Z directions. The melted material is extruded in thin strands and is deposited layer-by-layer in predetermined locations, where it cools and solidifies. Sometimes the cooling of the material is accelerated through the use of cooling fans attached on the extrusion head.
3. To fill an area, multiple passes are required (similar to coloring a rectangle with a marker). When a layer is finished, the build platform moves down (or in other machine setups, the extrusion head moves up) and a new layer is deposited. This process is repeated until the part is complete.

For the housing of 30 mm focal length lens of 18 mm diameter, SLA (Stereolithography) is used to get a smooth finish and accurate dimension. Stereolithography (SLA) is an additive manufacturing process that belongs to the Vat Photopolymerization family. In SLA, an object is created by selectively curing a polymer resin layer-by-layer using an ultraviolet (UV) laser beam.[33] The materials used in SLA

are photosensitive thermoset polymers that come in a liquid form. SLA is famous for being the first 3D Printing technology: its inventor patented the technology back in 1986. If parts of very high accuracy or smooth surface finish are needed, SLA is the most cost-effective 3D printing technology available. Best results are achieved when the designer takes advantage of the benefits and limitations of the manufacturing process. SLA has many common characteristics with Direct Light Processing (DLP), another Vat Photopolymerization 3D printing technology. For simplicity, the two technologies can be treated as equals. The working of SLA is as follows :

1. The build platform is first positioned in the tank of liquid photopolymer, at a distance of one-layer height for the surface of the liquid.
2. Then a UV laser creates the next layer by selectively curing and solidifying the photopolymer resin. The laser beam is focused in the predetermined path using a set of mirrors, called galvos. The whole cross-sectional area of the model is scanned, so the produced part is fully solid.
3. When a layer is finished, the platform moves at a safe distance and the sweeper blade re-coats the surface. The process then repeats until the part is complete.
4. After printing, the part is in a green, no-fully-cured state and requires further post processing under UV light if very high mechanical and thermal properties are required.

The liquid resin is solidified through a process called photopolymerization: during solidification, the monomer carbon chains that compose the liquid resin are activated by the light of the UV laser and become solid, creating strong unbreakable bonds between each other. The photopolymerization process is irreversible and there is no way to convert

the SLA parts back to their liquid form: when heated, they will burn instead of melting. This is because the materials that are produced with SLA are made of thermoset polymers, as opposed to the thermoplastics that FDM uses.

3.3 Design and further Implementation

Initially the design was with a single projector light, split by prism and then refocused with mirrors i.e light would be focused from two directions onto the object. The limitations of this design were requirement of very large mirrors and their mounting was mechanically not reliable. This design was further improved as it was very complex system. And also, these parts had to be custom made which was not feasible at the time.

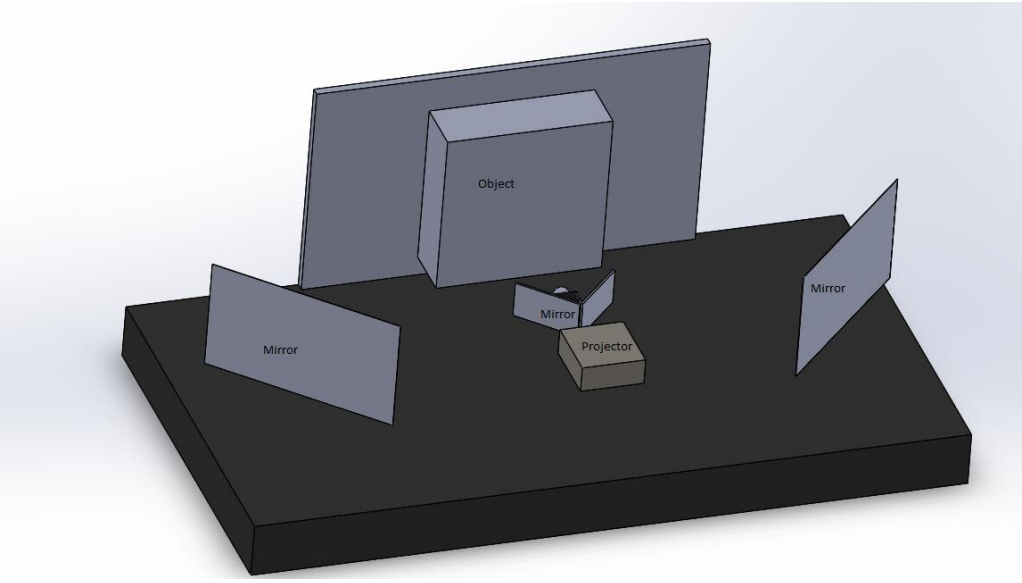

FIGURE 3. 6: This shows the Basic Initial design that was considered

Due to the gradual expansion of light from the projector “Lightcrafter 4500” this light had to be collimated in order to avoid decrease in the intensity of the fringes that would be projected onto the object. Due to this we have a constant magnification of the fringe pattern and nothing will be distorted when projected onto a plain surface, i.e the fringe pattern

generated, and the fringe pattern displayed would be same. A new set of lenses were required to make the system telecentric. The inbuilt lens system was removed and replaced with a lens of focal length 30mm and 18mm dia. A new housing for this lens had to be designed and 3-D printed. Lightcrafter 4500 comes with no housing of its own, so to integrate this into our system a housing was designed considering the ventilation of the projector as well. The light is collimated using a lens of 30 mm focal length at the starting point of the projector followed by a stop at 30 mm from the lens which would filter out only the parallel light rays from the projector. Then a lens of focal length 300 mm is used to enlarge this image from the projector, and this setup obtained a collimated light with zero magnification. The image was focused at a distance of 150 mm from the second lens. This whole system can be visualized from Figure 3.7, the 30 mm focal length plano-convex lens of 18 mm diameter is housed inside the projector using the 3D printed lens housing, the aperture is attached to the lens housing as well and the 4” lens on the right is placed using a lens mount on the optical base.

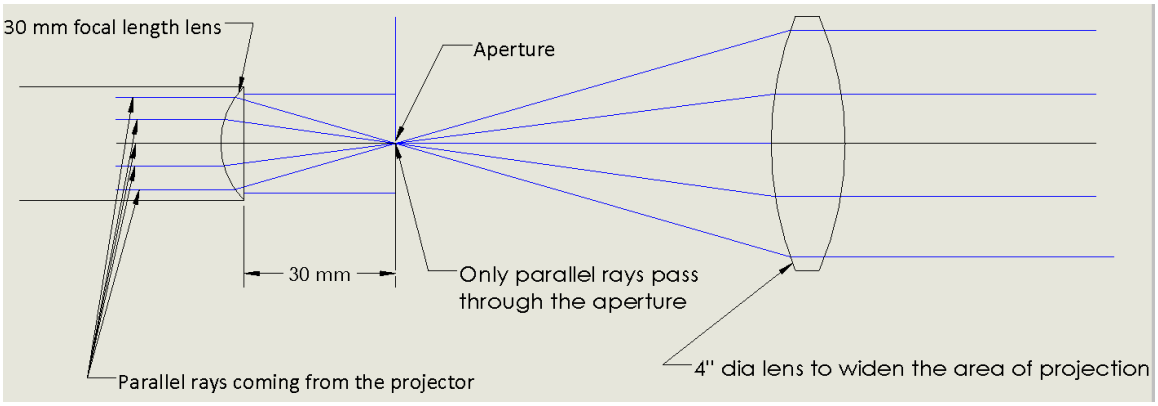

FIGURE 3. 7: Shows the basic geometry of the aperture allowing only parallel rays from the projector and we get a collimated light in the end.

This whole system is mounted vertically, and the object can be just placed on the base and measurements can be taken without having to specifically place the object at the correct distance. The starting CAD design is show in the Fig 3.8 and the hardware setup is shown in the Fig 3.9. The two projectors are aligned at an angle of 90^{o} to each other. This angle is chosen in order to eliminate the shadows and partially shiny surfaces . Smaller angles might not be sufficient to eliminate the shadows entirely i.e might leave shadows overlapping .

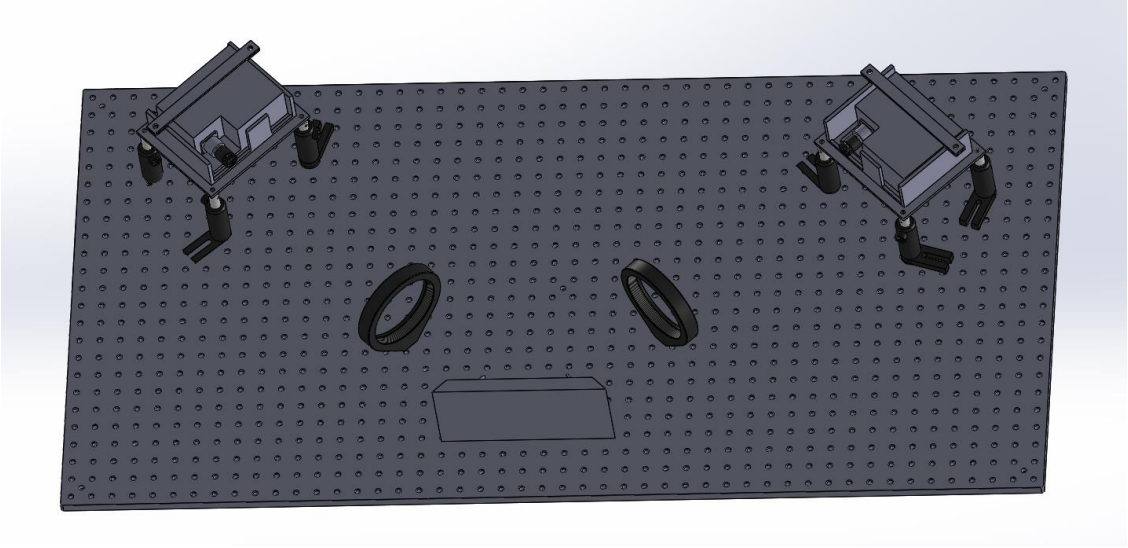

FIGURE 3. 8: CAD model of the Initial Design

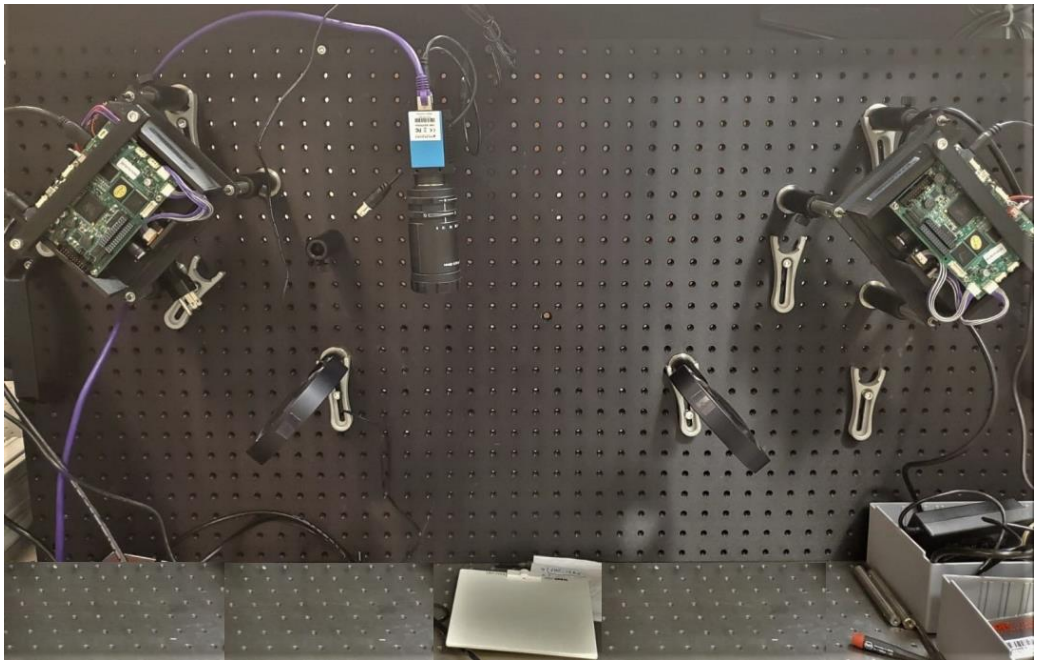

FIGURE 3. 9: shows the initial hardware setup along with the camera

CHAPTER 4: SOFTWARE

4.1 MATLAB

Throughout this experiment we use MATLAB to carry out all the readings and integrate with the camera and the projectors. The software is used to generate a checkerboard pattern to align the two DLP Lightcrafter 4500 projectors manually so that their projections superimpose with one another. The pattern is generated using repmat function in matlab. Once the projectors are aligned, we proceed to Gamma Calibration method discussed further in this chapter.

4.2 Gamma Correction

4.2.1 Introduction

Gamma correction is used to correct the differences between the way a camera captures content, the way a display displays content and the way our visual system processes light. Our eyes do not respond to light in the same way that a camera captures it. In basic terms, if twice the number of photons hit a digital image sensor, then the output voltage will be twice as big[34]. For the case of CMOS, CCD cameras, Digital Displays and Digital Projectors are built with gamma non-linearity. The entertainment industry deliberately causes the non-linearity to enhance the image for the human eye to understand the 3D world from a 2D image or screen. Simple linear images without any non-linearity would not look good on a screen. But to use projectors or displays for various Fringe projection techniques gamma correction should be addressed. With gamma pre-correction we can get an acceptable representation with only 8 bits. Photopic human vision characteristics can be approximated by a power law function. Correction of the signal output from the camera using this type of function ensures that not too many bits are allocated to brighter regions

where humans are less discriminating and more to darker regions, where they are more so. Video cameras therefore normally perform a non-linear mapping of illumination intensity to output value, providing a more uniform perceptual scale with finer increments for darker values. This is known as the Gamma Characteristic of the device as is described by the transfer function:

$$V = c_1 \Phi^{\gamma} + c_2 \qquad (4.1)$$

Where Φ is the luminous flux (normalized) and V is the value (voltage) of the signal, c_1 is the camera sensitivity and c_2 is an offset value. Figure 4.21 shows transfer characteristic plots for three gamma values,[34]. These values are typical of those used in modern TV systems. Figure 4.21 shows some corrected examples of an image at various gamma levels. Others also use the function $\frac{Sin^{-1}\phi}{\bar{T}an^{-1}\phi}$ shaped curve as a non-linearity in some industries. This choice depends on the manufacturer, however the simplest gamma non-linearity model is shown in Figure 4.1 and equation 4.1.

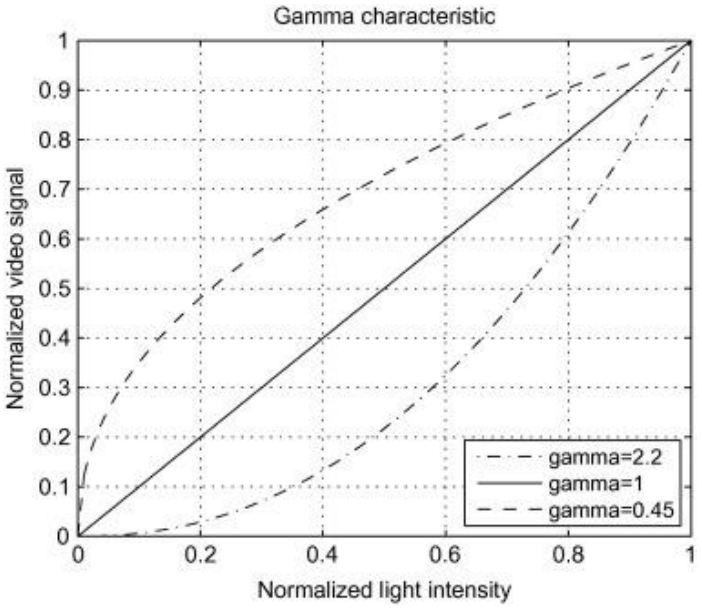

FIGURE 4. 1: Ideal Gamma Curves for $\gamma = \{0.45,1,2.2\}$

4.2.2 Methods used to calibrate Gamma

The projector used is Lightcrafter 4500 has to be compensated for their gamma offset which was made by the manufacturers to adjust for a general usage of the products. We send the signals from computer to projector in 8-bit format, due to this we know we have the color range from 0-255 (2^8 is 256 so there are 256 possible colors). This range is used for a single color in RGB from the darkest to the lightest color which can determine the gamma offset done by the manufacturers. We chose blue throughout the calibration and rest of the experiment. We can calibrate the gamma using two methods that we developed, will be discussed in the next subchapter. In both these methods the unnecessary data in the image captured is removed so that it does not alter any results.

In both the methods we developed, the idea is to find out the gamma curve and fit a polynomial to it and use an inverse polynomial which would compensate for the non-linearity and obtain the ideal curve. The first step in this process is to remove spatial Non-Uniformity. Spatial Non-Uniformity occurs mainly in projectors when the Intensity of the Brightness (I_{bright}) gradually decreases as we move away from the center. As the light has to travel more distance in the corners than the center causes this Non-Uniformity. So, we try to eliminate this first by using the data recorded from an image projected with an intensity of 255. Figure 4.2 shows the deformity when Intensity is plotted against in any one direction X or Y. The resulting curve would be similar to as shown in the figure. This is not ideal, and any Intensity is expected to be a straight line. The 125 could be any other Intensity between 0-255. And (I_{125}/I_{255})x255 will eliminate the spatial Non-Uniformity as both the Intensities will have the same Spatial Non-Uniformity factor, then this is scaled back to 255. This way any intensity value can be recorded without any spatial non-

uniformity as we have removed for the Intensity of 125 as an example. So now, the measured Image will be free of any kind of spatial Non-Uniformity.

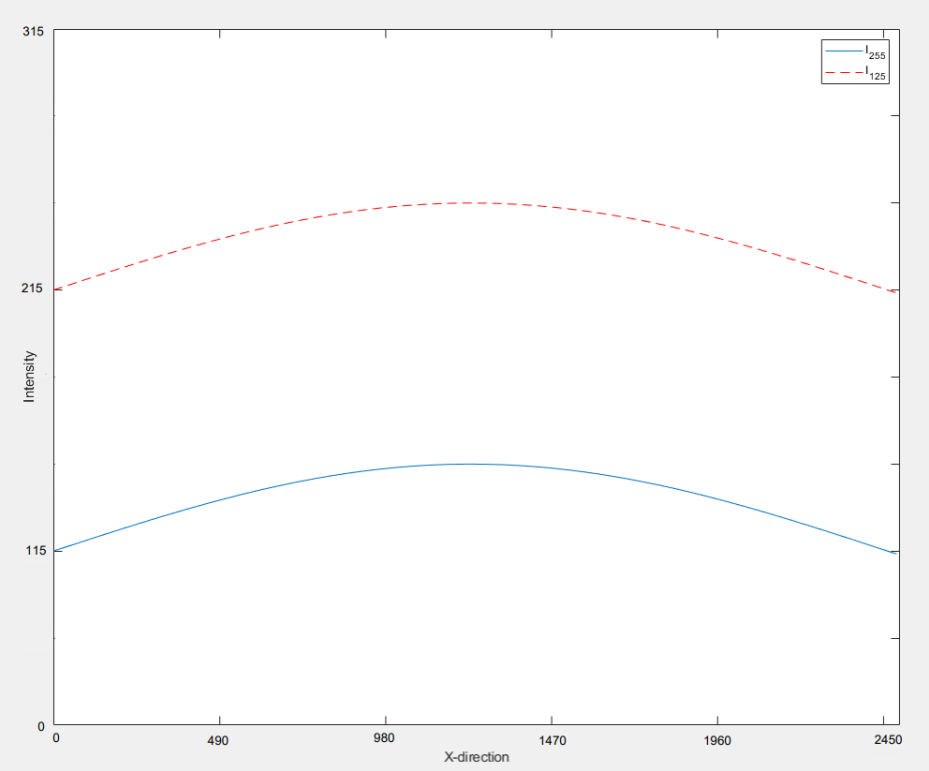

FIGURE 4. 2: Plot of Two different Intensities with spatial Non-Uniformity

Once this is done, the second step would be to send signals of greylevels and record and plot them. Once we have some data points recorded, we can use these to make an Inverse polynomial so that we know what function has to be sent in order to receive the function we intend to. Assuming we require a sine pattern of fringes to be recorded we should be sending a different function in order to receive a sine pattern. This different function can be calculated using interpolation using the inverse polynomial.

For example, if we assume, we need a sin(x) function to be received. And the polynomial to be a simple quadratic as shown below

$I_m = I_{send}^2$,

where I_m is the function measured by the camera and I_{send} is the function sent by the projector via computer.

If we need a sin(x) to be measured in this case, we need to send $\sqrt{sin(x)}$. This is the idea, but the polynomial can only be determined after sending and recording different grey levels and creating an inverse polynomial using them.

4.2.2.1 Using Greyscales from 0-255

In order to obtain the gamma values, we project an image with same value in all the pixels of the projector starting with 0 and record this and finally after 256 images are projected and recorded by the camera this can be plotted and we can see the offset created by the manufacturer. This method can be used with any system and the gamma offset can be determined accurately. In the figure 4.3 we can see that the gamma curve is clearly deviated from the ideal curve, this curve is of projector 1 and the curve is identical for projector 2 as well. The minor irregularities are due to fluttering effect of the projector which were normalized while taking readings however the raw data was not obtained smooth. This was the same in the two projectors used and was also tested with a different camera and this anomaly is entirely dependent on the type of projector used.

Gamma calibration is required if we are to obtain an accurate reading of an object. We can select few points of this calibration method and use them later on to estimate the size of an object to be measured. This method takes about 150 minutes of uninterrupted time to finish the calibration using the maximum number of frames possible and averaging them out to avoid any faulty readings.

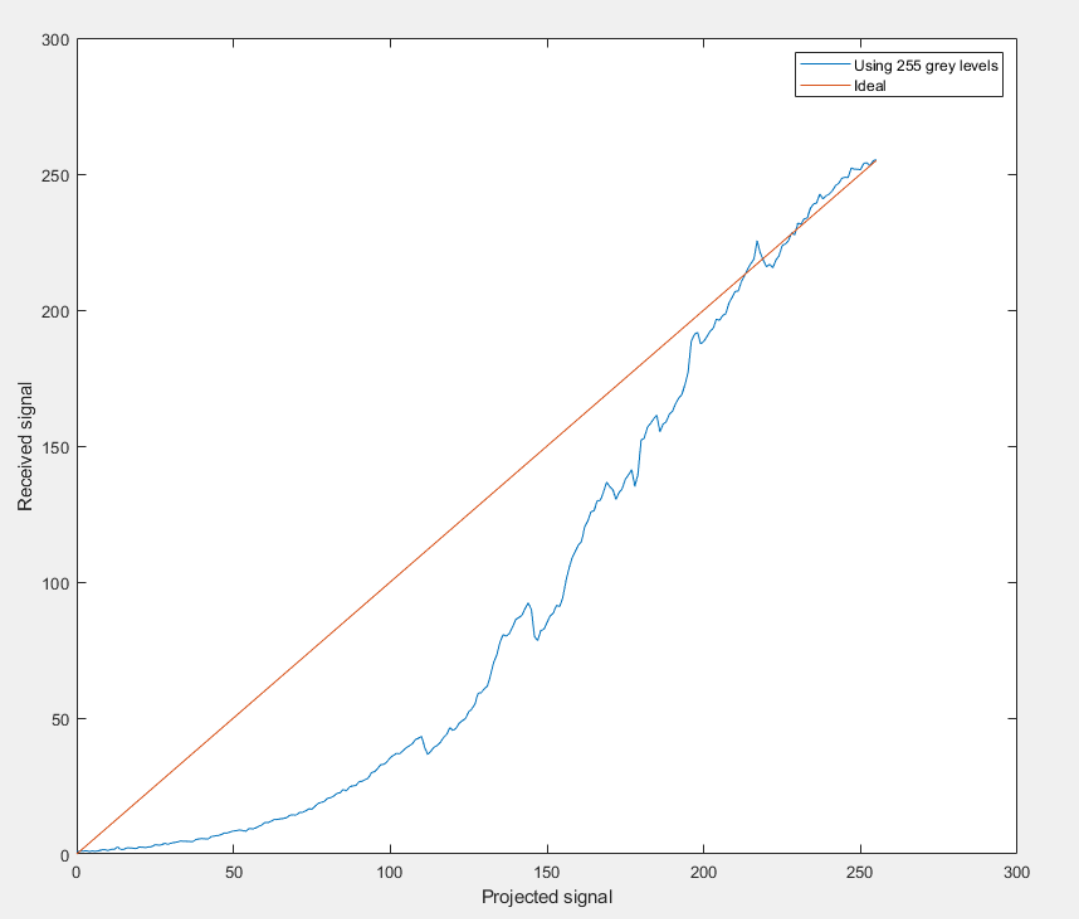

FIGURE 4. 3: Signal sent vs Received is plotted for projector 1

4.2.2.2 Using Patterns of different greyscales

In this method different patterns of greyscales ranging from 0-255 are used. That is a single image will contain different values of blue in a certain pattern. 8 particular greyscales are used in this between 0-255 not 256 shades of blue unlike the other method. Using this we obtain the recorded values for the 8 greyscales. This method consumed 14 minutes. In this method the code is designed in such a way that since we are using few greyscales, the inverse polynomial discussed before in this chapter can be accurately formed when the measured greylevels are equidistant. Since we cannot determine straight away what grey levels should be sent for obtaining equidistant greylevels when recorded, we start by

sending equidistant greylevels using linspace function in MATLAB. Once this is sent the code will check what points are recorded and recalculates the greylevels to be sent closer to make the recorded greylevels equidistant. This is an iterative process, finally the recorded values are obtained which are then used to get the inverse polynomial. This in-turn is used to find the function to be sent using interpolation as discussed before in this chapter. The code for this is complex because this is an iterative method but the time taken is relatively much faster.

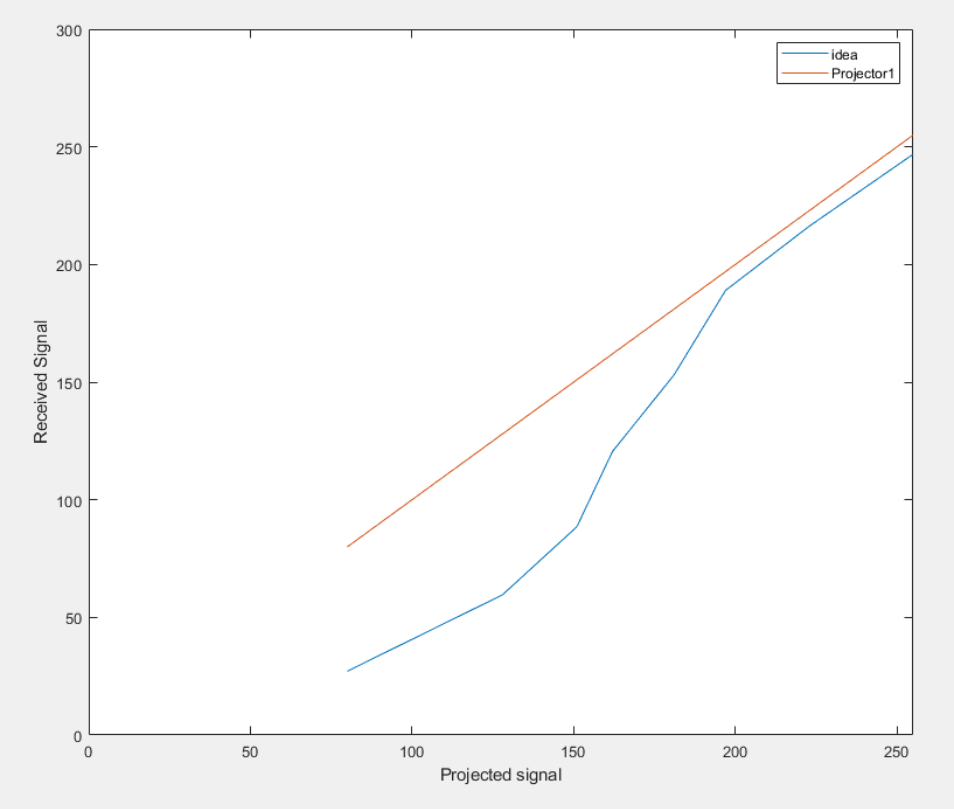

FIGURE 4. 4: Signal sent vs Received using the pattern method

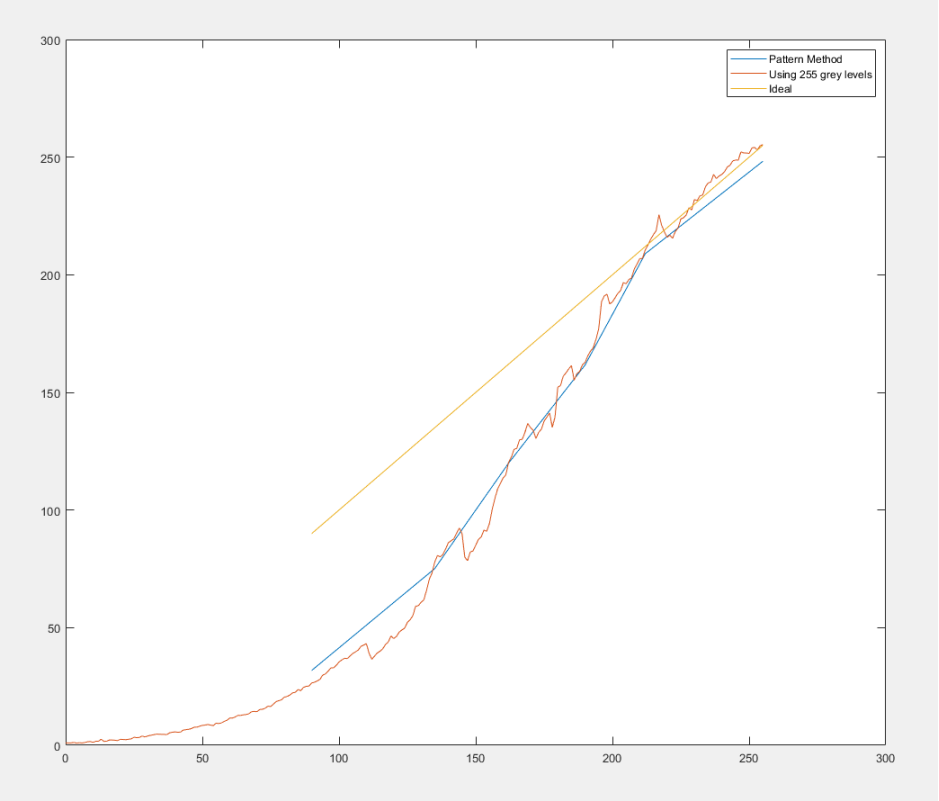

FIGURE 4. 5: Sent and Received Signal generated in two different methods

When the two methods are compared, they should be overlapping with each other, as the sent grey level(y-axis) and received grey level(x-axis) for both the methods should be same. We can observe this in Figure 4.5 that these readings overlap well with each other. The distortions in using 255 grey levels is due to the projector used as the Gamma in the camera is set to 1 (manually in code).

4.3 Main Absolute Phase

As discussed in chapter 2 the measured gamma is used to calculate the inverse polynomial which can give the desired function corresponding to a sine pattern that we intend to read. We use 20 frames and average this for each reading so that any flutter

in the projector or other anomalies would be eliminated by taking average of this. If we break this process of taking readings of a Fringe pattern, it would be as follows.

1. Generate N phase shifted frames for the generic Phase Shift Algorithm
2. Pre-code a nonlinear pattern for gamma compensation
3. Send to projector
4. Grab the phase shifted images
5. Repeat (1)-(3) for different fringe periods
6. Calculate phase at each period
7. Calculate absolute phase

In the first step we initialize all the required values for the camera settings and define the period for the sine pattern which will be projected onto the white background. A color channel has to be set to maintain continuity. For this experiment Blue color was chosen. Once the camera is ready to capture and we have initialized the sine pattern, we send this to the projector. We have used four periods of which the maximum period is just over the maximum resolution of the camera to obtain a good reading of the surface. Using fringe patterns of one axis (assuming we start with x-axis) we generate the sine pattern with four different periods and record this data in order to calculate Phase of X. Once all the data is recorded, we estimate the phase using the data in X axis. We have the phase, but this phase is currently wrapped. We use phase unwrapping algorithm which is based on the concept explained in chapter 2.5. Once the phase is unwrapped, we have the surface reading of one plane. In order to obtain the dimension of the complete surface, Phase in Y should be measured as well. With small adjustment the same process is followed to obtain Phase of Y- axis.

This process is repeated for the second projector as well. Our aim is to obtain a relation and an idea of how the volume varies for 1mm depth. So, we take 10 of these readings with 100μm apart. This will help us understand how a dual projector system works when these phase values are put together.

4.4 Experimental Results

The experimental setup is shown in Fig 4.7, with the hardware used which was explained in the previous chapters. When we measure the phase of an axis then multiply it with pi and divide by the period, we get the exact position of the pixel.

The equation for this is as follows:

$$Posi_x = AbsolutePhase_x \times Period/2\pi$$

Where $Posi_x$ is the position in X-direction that we can find from absolute Phase value of X and the same formula should be used to find Position of Y as well.

We have aligned the projectors manually so that there would be some offset which can be found using the pixel position. We are able to determine this shift as the camera orientation is undisturbed while measuring the phase of X and phase of Y from the two projectors. In the figure 4.6 the white board is the Z plane, the angle between the projectors is 50^o, it was not possible to go lesser due to the placement of the camera and lens. Previously in Figure 3.8 the angle between the projectors was 90^o , the same experiment is possible but the shift due to manual alignment of projectors would be huge and might not produce good results so , the lowest possible angle was chosen for taking the readings. We could have higher angle as well, but it is harder to align the projectors manually as the angle between the projectors increase. Ideally when we change the Z plane , we should observe that the light coming from two projectors will start moving away from each other.

This kind of shift would be linear and would vary gradually as we move the Z plane. We can see this in the Figure 4.6 where there are two planes and in plane 1 the light projected from two projectors are completely aligned and in plane 2 it looks as if the projected light from the two projectors have moved away from each other, which indicates that the pixel position of the projectors will have a big difference. So, we try to look at the results and understand how this shift between the two projectors behave while moving 100 μm in the Z-plane.

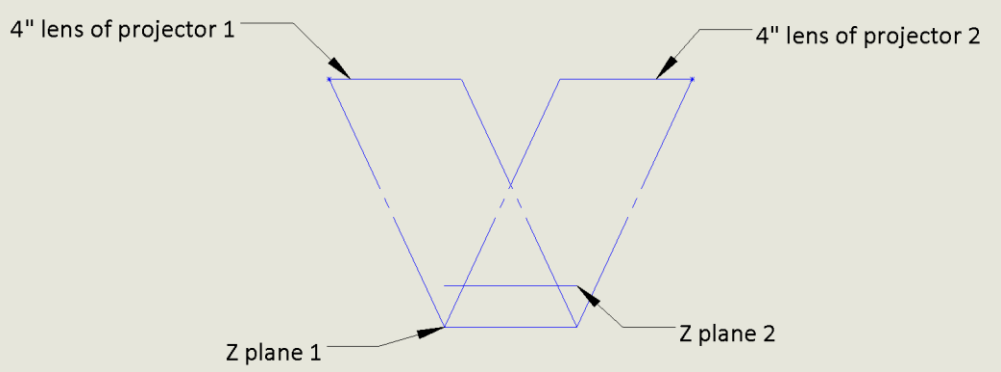

FIGURE 4. 6: Basic Geometry of two projectors and two Z planes

When we look at the Figure 4.8, it is simply the radial co-ordinate of X and Y positions. This makes it easier to look at the results and how the readings vary through Z-plane. The radial component is given by the following equation :

$$r^2 = \sqrt{x^2 + y^2}$$

This figure has radial components of two projectors marked as red (projector 1) and green (projector 2) and with 10 Z-planes spaced at 100μm up to 1mm. We can notice in this that as we move above through the Z-plane, the shift of fringe pattern is not visible as discussed before regarding the ideal case. Instead the data shows that as we move along upto 1mm, the exact shift (the shift due to manual alignment) between projector 1 and projector 2 are

quantified further below in this subsection. In Figure 4.9 we can see the raw data of positions of the two projectors indicated in red and green respectively that are plotted in normal cartesian co-ordinates with all 10 Z-planes.

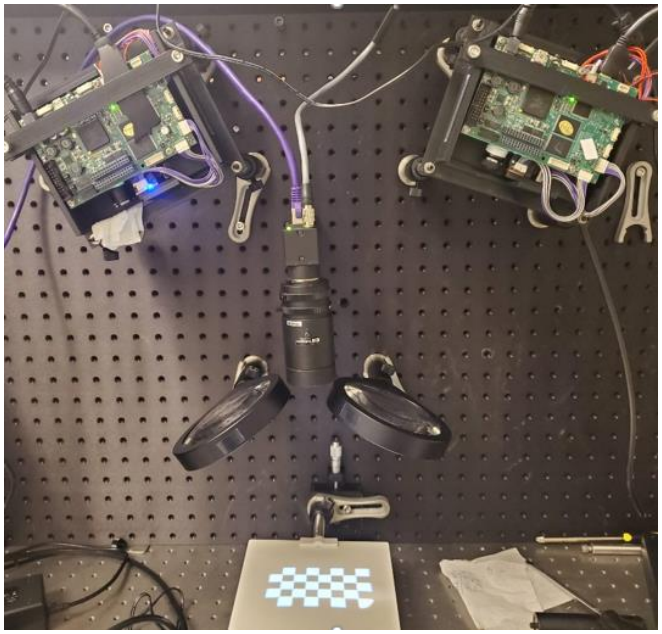

FIGURE 4. 7: Complete setup of the final system

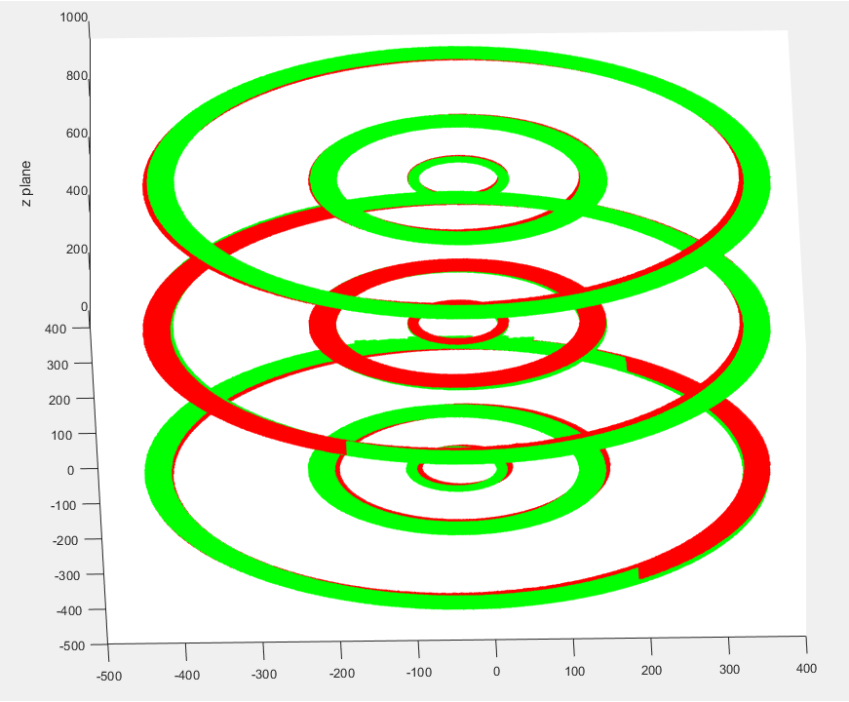

FIGURE 4. 8 : Radial component of the X,Y positions of 3 planes at 0,0.5,1 mm . Red color is of projector 1 and green is of projector 2

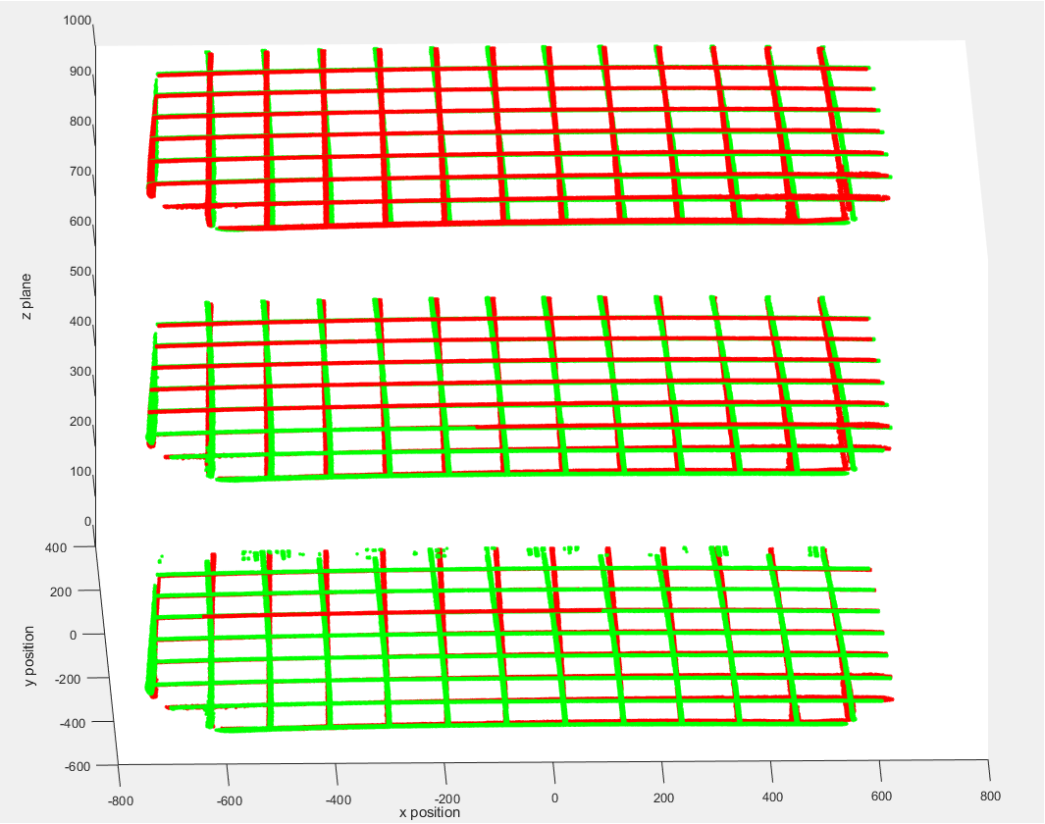

FIGURE 4. 9: Grid pattern of Phase data of X and Y positions of 3 planes along Z . Red color is of projector 1 and green is of projector 2

The Figure 4.8 and 4.9 which are variations of the same readings plotted as radial component of X and Y and the Figure 4.9 is the grid pattern of X and Y positions. The shift is noticeable as we go up through the Z plane. The green color corresponds to second projector which shifts to the right and the red color corresponds to the first projector which has shifted to the left. This Shift is measured clearly in Figure 4.10.

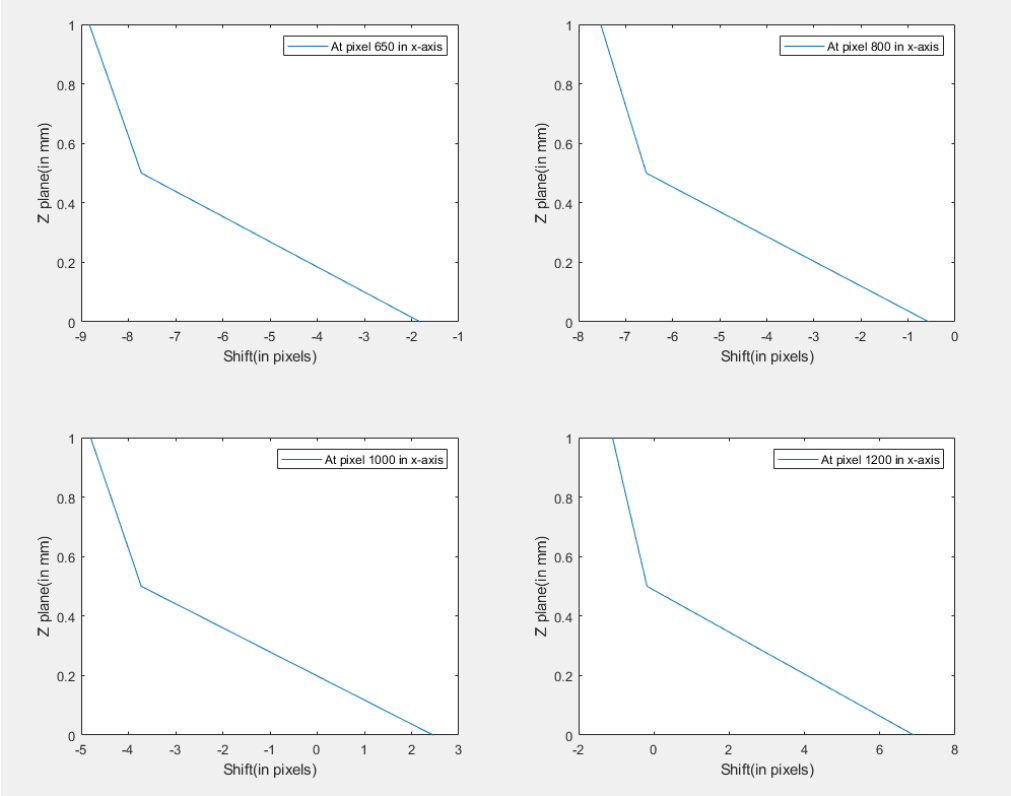

FIGURE 4. 10 : Shift at different pixels along center of y-axis through the Z plane

We can conclude this chapter as, by measuring the phase values of X and Y we can obtain the position of the pixels. By getting the position of the pixels we have used these to plot the radial component of X and Y positions. The three rings seen in

Figure 4.8 are made so that the shift of the two different projectors is clearly visible. In the similar manner we have plotted lines of X and Y to be able to clearly see how the shift occurs in cartesian co-ordinates as well. After looking at the results, we can clearly confirm that upto 1mm with 100μm apart in Z-direction the shift is 0.35431mm for one projector . This varies $\pm 0.02mm$ through different pixels. In figure 4.10 the shift in different pixels is plotted, the starting point of the shift is different due to manual alignment of the projectors. This alignment error is different at different pixels, but the shift through the Z

plane is consistent. So, this will enable us to measure volume of a surface accurately as we have determined the behavior of the shift when we move through the Z-plane.

A simple relationship between the shift and the distance between Z planes can be derived using the geometric relations from the figure 4.6, the equation is as follows

$$Shift = \left(\frac{Z}{tan \frac{180 - \theta}{2}} \right)$$

where Z is the distance between two Z planes and shift is the amount the light shifts as the Z plane is moved and θ is the angle between two projectors. So, for our case, Z is 1mm, (distance between the first Z plane and the last). θ is 50^{o}. Calculating using these values we can find that the shift is 0.44307mm theoretically. The shift we observed is 0.35431mm in practical situation. So, upto 1 mm experimentally the error in shift is 0.0888mm.

CHAPTER 5: CONCLUSIONS AND FUTURE WORKS

5.1 Conclusion

We have achieved two main goals in this research. The first one is an effective way to calibrate gamma, in two different methods which enables anyone to cross check the accuracy of their calibration . The second one, an experimental setup to determine how the dual projector system would behave within a volume of 1 mm.

In the gamma calibration, this is very essential as many devices are manufactured with a gamma offset for different applications. This gamma offset data is generally not available to the consumers and it is not easy to obtain this data from the manufacturer. So, the developed two methods could be used in wide range of fringe projection techniques. When we try to integrate this in additive manufacturing process to obtain real time data, the projector could be different and might be more specific to the kind of 3-D printer used. So, this gamma calibrations methods would eliminate the inaccuracies of data captured of the surface using Fringe Projection.

When we come to the experiment of measuring a simple Sine Fringe pattern projected by two different projectors. We have seen that as we move along the Z-plane the shift between the projectors due to their alignment is shifting through the Z-plane. This could only mean for certain that up to 1 mm the deviation between the projectors along the Z planes is the expected value that we obtained using basic trigonometric relations. This will lead to an accurate measurement of the surface which would be effective in eliminating any shadows due to the irregularities of the surface and also this shift data could help us in aligning the projectors more accurately. So, as a result when a 3-D printer

has this system integrated with it, it could give information of the surface as we move along the Z-plane when an object is manufactured. A further extension of this application would be, if the Fringe projector system is built on a movable base, then after 1mm of material is deposited, we can move the Fringe projector system 1mm and continue with the next layer of deposition. And we have the 3D model of the object being made, it would be possible to cross-check each layer manufactured with the 3D model. This application of Fringe projection system in 3-D printers would essentially save time and is cost effective by detecting faulty manufacturing as it happens. This would result in increasing efficiency and production rate of any manufacturing industry especially industries using Laser Powder Bed Fusion (a method of 3D printing). The Powder Bed Fusion process includes the following commonly used printing techniques: Direct metal laser sintering (DMLS), Electron beam melting (EBM), Selective heat sintering (SHS), Selective laser melting (SLM) and Selective laser sintering (SLS).

5.2 Future Works

There is a huge potential to carry this experiment further and obtain more data and analyze it. As we move along the Z-plane, we can increase the planes from 10 to 20 or more which would give a denser data for 1mm of thickness. Using this we can obtain a more accurate curve of the shift. It is possible to align these projectors digitally for a given plane, by changing the projected fringe patterns. In this way, a perfect alignment may be achieved. Now we are able to determine how the deviation behaves. Ideally the deviation should be linear in nature, but it is slightly non-linear. This could be due to small miscalibrations and the reason could be further explored. This can be directly integrated

with the 3D printer and get data of the Laser Power bed fusion process as each layer is manufactured.

FIGURE 5. 1 : Coin to be measured with surface glare

This can be further extended in the algorithm and process the data to make a co-phased profilometer where the data from the two projectors of the same area would be working together to eliminate shadows or surface glares. As we can see in the figure 5.1 data would be missing due to the light coming straight from the right side of the coin, which results in surface glare and some shadow.

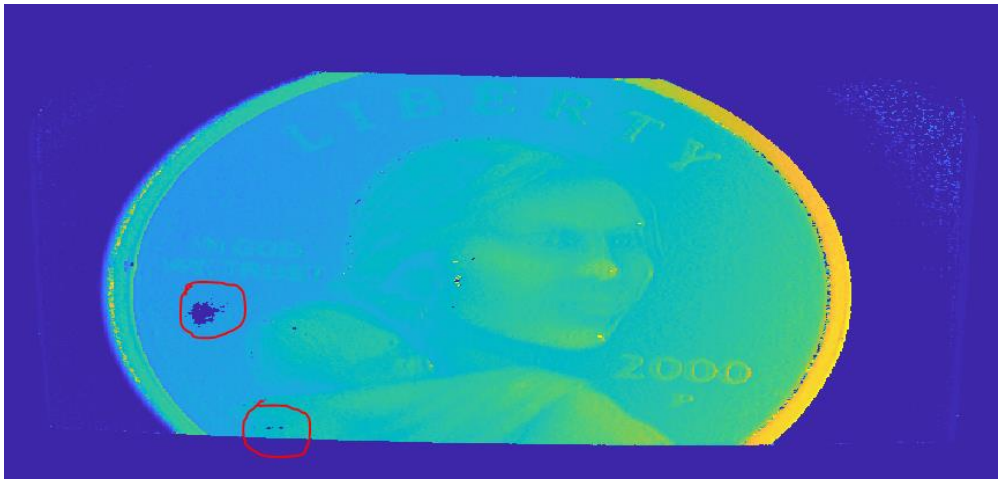

FIGURE 5. 2 : Phase map of a coin using projector 1

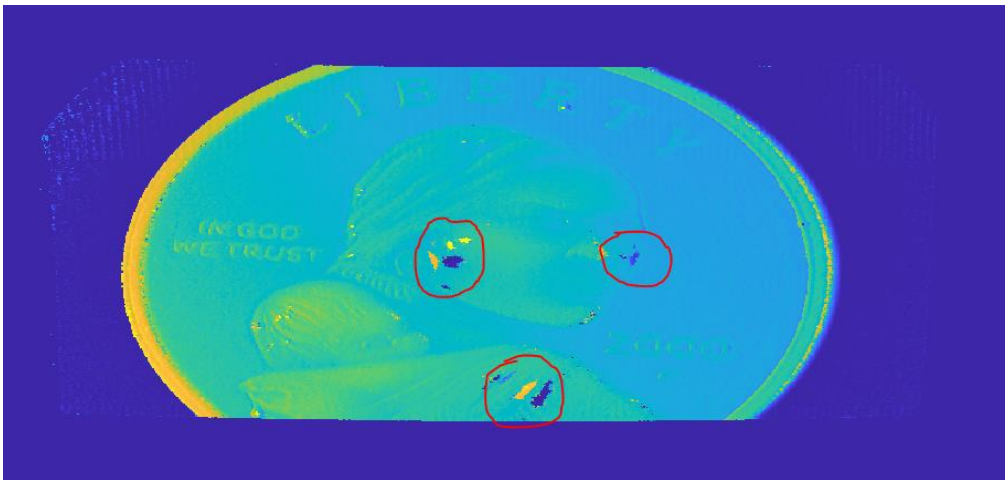

FIGURE 5. 3 : Phase map of a coin using projector 2

We measured a coin using the Fringe projection system that was developed and in Figure 5.2 we can notice some areas where the data is missing due to the projector's angle of incident of light onto the object and in Figure 5.3, we can see data missing at different points. Using Co-phasing Fringe projection techniques which is more robust algorithm. We can estimate the phase using the intensity data from both projectors at the same time without any need for stitching where several other errors occur. We can create an algorithm that uses this system and co-phased data to detect system drifts and performs automatic recalibration when necessary.

REFERENCES

[1] T. Wohelers, “Wohlers Report 2013: Additive Manufacturing and 3D Printing State of the Industry,” *Wohlers Rep. 2013*, 2013.

[2] D. Bue, D. Chiffre, H. Nørgaard, and D. B. Pedersen, “Additive Manufacturing Multi Material Processing and Part Quality Control Author,” p. 247, 2013.

[3] Z. J. Geng, “Rainbow three-dimensional camera: new concept of high-speed three-dimensional vision systems,” *Opt. Eng.*, 2006.

[4] T. T. Li, H. Y. Zhang, and J. Geng, “Geometric calibration of a camera-projector 3D imaging system,” in *International Conference Image and Vision Computing New Zealand*, 2010.

[5] D. J. Bone, H.-A. Bachor, and R. J. Sandeman, “Fringe-pattern analysis using a 2-D Fourier transform,” *Appl. Opt.*, 1986.

[6] A. M. Valkenberg, R J; McIvor, “Accurate 3D measurement using a structured light system,” *Image Vis. Comput.*, 1998.

[7] J. L. Posdamer and M. D. Altschuler, “Surface measurement by space-encoded projected beam systems,” *Comput. Graph. Image Process.*, 1982.

[8] E. Trucco and A. Verri, “Introductory Techniques for 3D Computer Vision,” *Englewood Cliffs, NJ, itd: Prentice Hall, str*. 1998.

[9] P. Barradas, “3D Surface Shape Information from Fringe Projection Techniques,” no. November, pp. 1–10, 2017.

[10] P. G. Cielo, “Optical techniques for industrial inspection.” Academic press Inc., 1988.

[11] Y. Liu, “Accuracy improvement of 3D measurement using digital fringe projection,” p. 112, 2011.

[12] S. Zhang, “Measurement,” no. May, 2005.

[13] a Thesis, “A Fringe Projection System for Measurement of Condensing Fluid Films in Reduced Gravity,” *Camera*, 2005.

[14] H. Gross, “Metrology and Sensing,” 2017.

[15] M. Halioua and H. C. Liu, “Optical three-dimensional sensing by phase measuring profilometry,” *Opt. Lasers Eng.*, pp. 185–215, 1989.

[16] D. Nobis and C. M. Vest, “Statistical analysis of errors in holographic interferometry,” *Appl. Opt.*, 1978.

[17] T. R. Judge and P. J. Bryanston-Cross, “A review of phase unwrapping techniques in fringe analysis,” *Opt. Lasers Eng.*, 1994.

[18] E. Zappa and G. Busca, “Comparison of eight unwrapping algorithms applied to Fourier-transform profilometry,” *Opt. Lasers Eng.*, 2008.

[19] P. Jia, J. Kofman, and C. English, “Real-time full-field 3-D surface-shape measurement using off-the-shelf components and a single processor,” *3DIM 2007 - Proc. 6th Int. Conf. 3-D Digit. Imaging Model.*, no. December, pp. 382–389, 2007.

[20] P. Jia, J. Kofman, and C. English, “Multiple-step triangular-pattern phase shifting and the influence of number of steps and pitch on measurement accuracy,” *Appl. Opt.*, 2007.

[21] C. Waddington and J. Kofman, “Analysis of measurement sensitivity to illuminance and fringe-pattern gray levels for fringe-pattern projection adaptive to ambient lighting,” *Opt. Lasers Eng.*, 2010.

[22] J. Kofman, “Two-step triangular-pattern phase-shifting method for three-dimensional object-shape measurement,” *Opt. Eng.*, 2007.

[23] “Multilevel two-dimensional phase unwrapping Iddit Shalem,” 2007.

[24] C. Zuo, L. Huang, M. Zhang, Q. Chen, and A. Asundi, “Temporal phase unwrapping algorithms for fringe projection profilometry: A comparative review,” *Opt. Lasers Eng.*, 2016.

[25] O. F. Technology, “Shape Measurements using Shape Measurements using Temporal,” 2000.

[26] J. Burke, T. Bothe, W. Osten, and C. F. Hess, “Reverse engineering by fringe projection,” in *Proc.SPIE*, 2002, vol. 4778.

[27] M. Zervas, C. Furlong, E. Harrington, and I. Dobrev, “3D Shape Measurements with High-Speed Fringe Projection and Temporal Phase Unwrapping,” in *Conference Proceedings of the Society for Experimental Mechanics Series*, vol. 5, 2011, pp. 235–241.

[28] M. Servin, G. Garnica, and J. M. Padilla, “Co-phased 360-degree profilometry of discontinuous solids with 2-projectors and 1-camera,” vol. 344, no. 1999, p. LTh2B.2, 2014.

[29] L. J. Hornbeck, “Current status of the digital micromirror device (DMD) for projection television applications,” 2002.

[30] J. M. Younse, “Mirrors on a chip,” *IEEE Spectr.*, 1993.

[31] J. Kollataj, “Additive Manufacturing (3D Printing)-A Potential Future for Tennis Racket Production Could 3D Printing / Additive Manufacturing eventually replace the current manufacturing method?,” 2016.

[32] Alkaios Bournias Varotsis, “Introduction to FDM 3D printing.” [Online]. Available: https://www.3dhubs.com/knowledge-base/introduction-fdm-3d-printing.

[33] Alkaios Bournias Varotsis, “Introduction to SLA 3D Printing.” [Online]. Available: https://www.3dhubs.com/knowledge-base/introduction-sla-3d-printing.

[34] A. Measurement, C. Space, and D. R. Bull, “Learn more about Gamma Correction Digital Picture Formats and Represen- tations,” 2014.